Received: 17 February 2020 | Revised: 26 April 2020 | Accepted: 14 May 2020

DOI: 10.1002/cne.24959

RESEARCH ARTICLE

JCN RESEARCH IN SYSTEMS NEUROSCIENCE THE JOURNAL OF COMPARATIVE NEUROLOGY WILEY

Dynamics of the fragile X mental retardation protein correlates with cellular and synaptic properties in primary auditory neurons following afferent deprivation

Xiaoyan Yu[1] | Xiaoyu Wang[1,2] | Hitomi Sakano[3,4] | Diego A. R. Zorio[1] | Yuan Wang[1]

[1]Program in Neuroscience, Department of Biomedical Sciences, Florida State University College of Medicine, Tallahassee, Florida, USA

[2]Division of Histology & Embryology, Key Laboratory for Regenerative Medicine of the Ministry of Education, Medical College, Jinan University, Guangzhou, China

[3]Department of Otolaryngology, Bloedel Hearing Research Center, University of Washington, Seattle, Washington, USA

[4]Department of Otolaryngology, University of Rochester, Rochester, New York, USA

Correspondence
Yuan Wang, 1115 West Call Street, Florida State University, Tallahassee, FL 32306.
Email: yuan.wang@med.fsu.edu

Funding information
United States - Israel Binational Science Foundation, Grant/Award Number: 2015087; National Institute on Deafness and Other Communication Disorders, Grant/Award Numbers: DC000018, R01DC13074, R21DC17267

Peer Review
The peer review history for this article is available at https://publons.com/publon/10.1002/cne.24959.

Abstract

Afferent activity dynamically regulates neuronal properties and connectivity in the central nervous system. The Fragile X mental retardation protein (FMRP) is an RNA-binding protein that regulates cellular and synaptic properties in an activity-dependent manner. Whether and how FMRP level and localization are regulated by afferent input remains sparsely examined and how such regulation is associated with neuronal response to changes in sensory input is unknown. We characterized changes in FMRP level and localization in the chicken nucleus magnocellularis (NM), a primary cochlear nucleus, following afferent deprivation by unilateral cochlea removal. We observed rapid (within 2 hr) aggregation of FMRP immunoreactivity into large granular structures in a subset of deafferented NM neurons. Neurons that exhibited persistent FMRP aggregation at 12–24 hr eventually lost cytoplasmic Nissl substance, indicating cell death. A week later, FMRP expression in surviving neurons regained its homeostasis, with a slightly reduced immunostaining intensity and enhanced heterogeneity. Correlation analyses under the homeostatic status (7–14 days) revealed that neurons expressing relatively more FMRP had a higher capability of maintaining cell body size and ribosomal activity, as well as a better ability to detach inactive presynaptic terminals. Additionally, the intensity of an inhibitory postsynaptic protein, gephyrin, was reduced following deafferentation and was positively correlated with FMRP intensity, implicating an involvement of FMRP in synaptic dynamics in response to reduced afferent inputs. Collectively, this study demonstrates that afferent input regulates FMRP expression and localization in ways associated with multiple types of neuronal responses and synaptic rearrangements.

KEYWORDS

afferent influence, apoptosis, auditory processing, endbulb synapses, fragile X syndrome, homeostatic synaptic plasticity, protein synthesis, RRID: AB_143162, RRID: AB_143165, RRID: AB_2492094, RRID: AB_2533969, RRID: AB_2572212, RRID: AB_476743, RRID: AB_887717, RRID: AB_94805

1 | INTRODUCTION

Fragile X mental retardation protein (FMRP) is a polyribosome-associated RNA-binding protein that binds to a diverse group of mRNAs and regulates their stability, transport, and translation (Darnell et al., 2011). Clinically, loss of FMRP due to the trinucleotide repeat expansion in the *Fmr1* gene leads to Fragile X syndrome (FXS), the most common inherited cause of autism and intellectual disability (Bassell & Warren, 2008; Penagarikano, Mulle, & Warren, 2007). Loss-of-function studies in animal models reveal compromised brain dynamics following FMRP downregulation. For example, FMRP is required in experience-dependent neural plasticity across sensory modalities. Young dendritic spines in cortical pyramidal neurons are sensitive to modulation of sensory experience in wildtype but not *Fmr1* knockout mice (Pan, Aldridge, Greenough, & Gan, 2010). Tonotopic auditory representation in the auditory cortex is normally regulated by a pattern of acoustic stimulation during development, but this regulation is weakened after FMRP loss (H. Kim, Gibboni, Kirkhart, & Bao, 2013). Similarly, the tonotopic distribution of Kv3.1b and its modification by sound stimulation in the medial nucleus of the trapezoid body (MNTB) are disrupted in *Fmr1* knockout mice (Strumbos, Brown, Kronengold, Polley, & Kaczmarek, 2010).

However, the dynamics of FMRP in response to changes in afferent inputs is not fully understood under either pathological or physiological conditions. Several studies have established a relationship between FMRP expression and sensory experience in sensory neurons. Extended exposure to an enriched environment or light exposure to dark-reared animals leads to increased FMRP levels in the visual cortex (Gabel et al., 2004; Irwin et al., 2000, 2005). FMRP upregulation is also observed in the somatosensory cortex as a result of unilateral whisker stimulation or in the motor cortex following repeated training on motor skill tasks (Irwin et al., 2000; Todd & Mack, 2000). Other studies demonstrate links between changes in FMRP level and phosphorylation and synaptic transmission through ionotropic and metabotropic glutamate receptors (Bartley et al., 2016; Ceman et al., 2003; Mazroui et al., 2003; Todd, Malter, & Mack, 2003; Weiler et al., 1997). It remains unknown whether FMRP is associated with different neuronal responses when afferent input is compromised, a pathological condition with clinical relevance.

In this study, we investigated how excitatory afferent input regulates neuronal FMRP through a systematic characterization of the time course of FMRP changes in primary cochlear neurons following afferent deprivation. In the auditory system, hearing impairment at young ages leads to neuronal loss and long-term alterations of neuronal properties and connectivity (Clarkson, Antunes, & Rubio, 2016; Hagerman et al., 2017; Kotak et al., 2005; Ocak, Eshraghi, Danesh, Mittal, & Eshraghi, 2018; Takesian, Kotak, & Sanes, 2009). Unilateral cochlea removal provides a powerful approach for examining the effect of excitatory afferent deprivation or hearing loss on the central nervous system, particularly in the mammalian ventral cochlear nucleus (VCN) and its avian analogue, the nucleus magnocellularis (NM). This manipulation, when performed in young animals, leads to 20–40% of neuronal cell death in the VCN and NM within 2 days, and altered cellular properties of the remaining neurons (Born & Rubel, 1985, 1988; Francis & Manis, 2000; Hashisaki & Rubel, 1989; Mostafapour, Cochran, Del Puerto, & Rubel, 2000; Sie & Rubel, 1992; Steward & Rubel, 1985; Tierney, Russell, & Moore, 1997). The presence of the two cell populations provides an opportunity to characterize FMRP dynamics and its potential involvement in cell survival and alterations. Using immunocytochemistry, we have previously shown that VCN and NM neurons normally express high levels of FMRP (Beebe, Wang, & Kulesza, 2014; Y. Wang et al., 2014; Zorio, Jackson, Liu, Rubel, & Wang, 2017). In this study, we characterized changes in FMRP immunoreactivity in the afferent-deprived NM using the NM on the other side of the brain as a within-animal control. A major goal of this study was to determine whether rapid changes in FMRP expression and localization are associated with cell death and survival within the first 2 days following afferent deprivation. The second goal was to examine the long-term relationship of FMRP to cellular and synaptic properties of surviving neurons after they regain cellular homeostasis at 1–2 weeks following afferent deprivation. Our results identify new forms of FMRP dynamics and uncover novel correlations between FMRP and cellular and synaptic properties with intact or reduced afferent inputs.

2 | MATERIALS AND METHODS

2.1 | Animals

This study was performed on White Leghorn chicken hatchlings (*Gallus gallus domesticus*) of both sexes. Fertilized eggs were purchased from the Charles River Laboratories (Wilmington, MA) and incubated in a Florida State University vivarium. All procedures were approved by the Florida State University Institutional Animal Care and Use Committee and conducted in accordance with the National Institutes of Health Guide for the Care and Use of Laboratory Animals.

2.2 | Unilateral cochlea removal

Cochlea were removed from the right side of 3–10 day old chicken hatchlings (n = 40 animals). The cochlea removal procedure was the same as described previously (Born & Rubel, 1985; Y. Wang, Cunningham, Tempel, & Rubel, 2009). Animals were anesthetized with a mixture of 40 mg/kg ketamine and 12 mg/kg xylazine. The tympanic membrane was punctured and the columella was removed to expose the oval window by using a pair of fine tweezers. The basilar papilla (the avian cochlea) was removed through the oval window, floated on water, and examined under a microscope to ensure complete removal. The procedure resulted in an immediate and complete elimination of excitatory afferent input to the auditory nerve while leaving the ganglion cell bodies intact (Born, Durham, & Rubel, 1991; Born & Rubel, 1985). Following the surgery, animals were allowed to survive for 2 hr (n = 5), 4 hr (n = 5), 6 hr (n = 5), 12 hr (n = 5), 24 hr (n = 5), 48 hr (n = 4), 96 hr (n = 4), and 1–2 weeks (n = 7). Five additional animals that did not undergo surgery served as controls.

2.3 | Immunocytochemistry

Experimental and control animals were deeply anesthetized and transcardially perfused with 0.9% saline followed by 4% paraformaldehyde in 0.1 M phosphate buffer (PB). Brains were removed from skulls, postfixed overnight, and transferred to 30% sucrose in PB for cryoprotection. Brains were then sectioned coronally at 25 μm on a freezing sliding microtome and collected in phosphate-buffered saline (PBS). Attention was made to cut symmetrically so that the left and right NMs in the same section were at comparable locations along the rostrocaudal axis. Alternate series of sections were used for immunocytochemistry as previously described (McBride, Rubel, & Wang, 2013; X. Wang, Zorio, Schecterson, Lu, & Wang, 2018). Briefly, free-floating sections were incubated with primary antibody solutions diluted in PBS with 0.3% Triton X-100 and 5% normal goat serum for two overnights at 4°C. After washing with PBS, the sections were incubated with Alexa 488 goat anti-rabbit and Alexa 568 goat anti-mouse secondary antibodies (1:500; Thermo Fisher Scientific, Waltham, MA; RRID: AB_143165 and RRID: AB_143162) in PBS for 6 hr at room temperature. Nuclear and cell body counterstains were performed together with the incubation of secondary antibodies using DAPI and NeuroTrace 640/660 (1:1000; Thermo Fisher Scientific; RRID: AB_2572212). After washing, sections were mounted on gelatin-coated slides and coverslipped with Fluoromount-G mounting medium (Southern Biotech, Birmingham, AL).

For peroxidase staining of FMRP, after primary antibody incubation, sections were incubated in a biotinylated IgG antibody (1:200; Thermo Fisher Scientific; RRID: AB_2533969) diluted in PBS with 0.3% Triton X-100 for 1 hr at room temperature. After washing in PBS, sections were incubated in avidin-biotin-peroxidase complex solution (ABC Elite kit; Vector Laboratories, Burlingame, CA) diluted 1:100 in PBS with 0.3% Triton X-100 for 1 hr at room temperature. Sections were then washed in PBS and incubated for 3–5 min in 0.045% 3-3-diaminobenzidine (MilliporeSigma, Burlington, MA) with 0.03% hydrogen peroxide in PB. Sections were mounted on gelatin-coated slides and dehydrated, cleared, and coverslipped with Permount mounting medium (Thermo Fisher Scientific).

2.4 | Primary antibodies

A rabbit polyclonal antibody against chicken FMRP was custom-made by Pierce Biotechnology (a part of Thermo Fisher Scientific). The

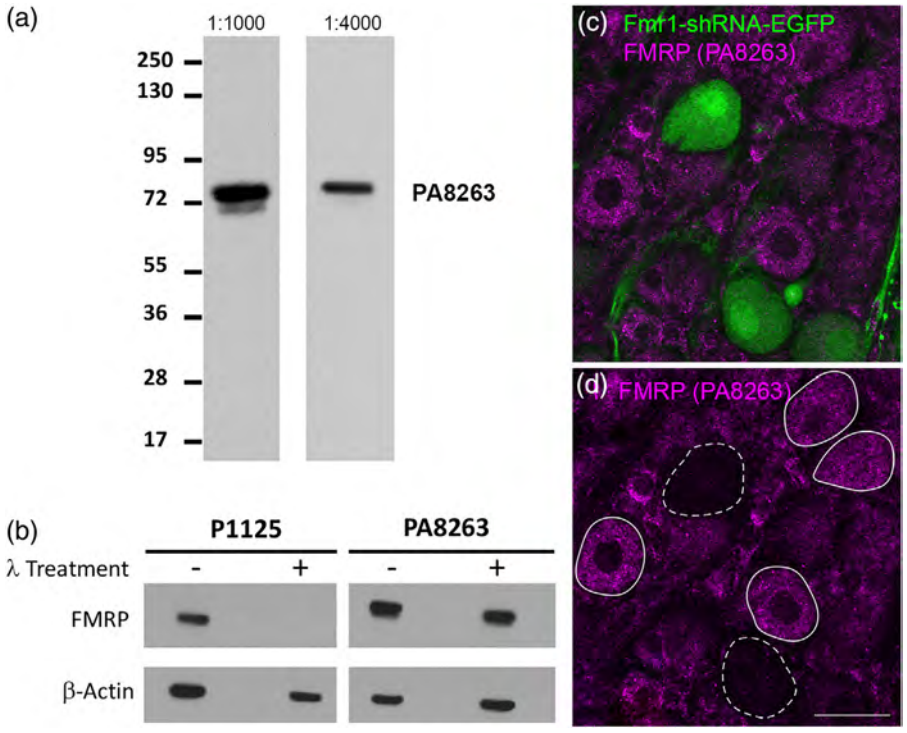

FIGURE 1 Antibody validation of anti-FMRP (PA8263) and anti-p-FMRP (P1125). (a) Western blot assay on homogenized chick dorsocaudal brainstem samples. Molecular weight standards (left) were used to determine relative sizes of labeled proteins. Anti-FMRP (PA8263) detects a single band of just above of the 72 kDa at 1:1000 (left) and 1:4000 (right) antibody concentrations. (b) Anti-FMRP (PA8263) detects the same band regardless of phosphatase treatment. Anti-p-FMRP (P1125) detects a band of the same molecular weight under normal conditions but is absent following phosphatase treatment. β-Actin was used for loading control. (c, d) Immunostaining of anti-FMRP (PA8263) following genetic knockdown of FMRP expression in NM neurons. Images were taken from a E19 chicken embryo that received *in ovo* electroporation of a *Fmr1*-shRNA with an EGFP reporter (X. Wang et al., 2018). Transfected NM neurons (green; dashed circles) show reduced FMRP immunostaining as compared to non-transfected neurons (magenta; solid circles). Scale bar = 20 μm in d (applies to c,d) [Color figure can be viewed at wileyonlinelibrary.com]

immunogen was a synthetic peptide (KGNDEQSRTDNRQRNSRDAK), designed near the C-terminus of the chicken full length protein, conjugated to keyhole limpet hemocyanin protein. The specificity of this antibody was tested using western blot and a genetic knock down method (see Results and Figure 1). The antibody was used at 1:1000 for immunocytochemistry; this optimal antibody concentration was determined through a series of concentration tests to avoid floor or ceiling truncation.

Monoclonal Y10B antibody for ribosomal RNA was a gift from Dr. Edwin Rubel (University of Washington, Seattle, WA). This antibody was originally generated from a genetic mouse model of autoimmune disease by Dr. Joan Steitz at Yale University (Lerner, Lerner, Janeway Jr., & Steitz, 1981). The Y10B antibody immunoprecipitates whole ribosomes as well as all sizes of phenol-extracted rRNA, indicating that it recognizes a nucleic acid motif common to many rRNAs (Garden, Canady, Lurie, Bothwell, & Rubel, 1994; Lerner et al., 1981).

All other primary antibodies were purchased commercially. This includes the monoclonal mouse anti-synaptosome associated protein 25 (SNAP25; MiliporeSigma, #MAB 331; RRID: AB_94805); the monoclonal mouse anti-gephyrin (Synaptic Systems, Göttingen, Germany; #147011; RRID: AB_887717); the monoclonal mouse anti-beta-Actin (MilliporeSigma, #A5316; RRID:AB_476743); and the polyclonal rabbit anti-phosphorylated FMRP, Ser499 (PhosphoSolutions, Aurora, CO; #P1125; RRID: AB_2492094).

2.5 | *In ovo* electroporation

To downregulate FMRP levels in NM neurons, we introduced a shRNA directed against chicken *Fmr1* into NM precursors via *in ovo* electroporation. The shRNA was cloned into a transposon-based vector system with a *Tol2* vector containing doxycycline regulatory components and an EGFP reporter. The shRNA construct design and *in ovo* electroporation were described in our previous study (X. Wang et al., 2018). Briefly, eggs were incubated until embryonic day 2 (E2). The plasmid was injected into the lumen of neural tube at the rhombomere 5/6 level, which contains NM neuron precursors. A platinum bipolar electrode was placed to the two sides of the neural tube, delivering short electrical pulses (4 pulses at 20 V with 30 ms duration and 10 ms between pulses). Following electroporation, the eggs were returned to the incubator. At E8, 50 μl of 1 mg/ml doxycycline (MilliporeSigma) was added onto the chorioallantoic membrane to trigger the transcription of shRNAs and EGFP. The administration was performed again every other day to maintain the expression before tissue dissection at E19.

2.6 | Western blot

Protein samples were harvested from flash frozen chicken brainstem tissue. Samples were homogenized in EDTA buffer (62.5 mM Tris–HCl pH 6.8, 2% SDS, 10% Glycerol, 5% β-ME, 10 mM EDTA) using the Ultra-Turrax® T10 homogenizer (IKA® Works, Inc., Wilmington, NC). Fifty microgram (50 μg) of protein lysate in SDS buffer (2% SDS, 50 mM Tris pH 7.6, 5% glycerol, and 0.025% bromophenol blue) was incubated at 70°C for 10 min, resolved in NuPAGE 4–12% Bis-Tris Gels (Life Technologies, Carlsbad, CA), and then transferred onto PDVF membranes (GE Healthcare, Chicago, IL). The PVDF membranes were washed for 5 min in Tris-buffered saline with 0.05% Tween-20 (TBS-T). Phosphatase treatment was carried out using the lambda phosphatase kit (P9614; MilliporeSigma, St. Louis, MO) following manufacturer's instructions. After blocking in 5% milk in TBS-T for 30 min at room temperature, membranes were probed against the primary antibodies overnight at 4°C in 1% milk in TBS-T. Specific secondary HRP-conjugated antibodies were used at 1:2500 dilution (Santa Cruz Biotechnology, Inc., Dallas, TX) and blots were developed with SuperSignal™ West Pico Chemiluminescent Substrate (Thermo Fisher Scientific) and exposed to X-ray film.

2.7 | Quantification of changes in FMRP intensity

Four to five animals were used for each experimental and control group. For each animal, fluorescent FMRP immunostaining and NeuroTrace staining were performed on two coronal sections: one at ~50% and the other at 75% distance from the caudal NM, representing the intermediate and rostral regions of NM, respectively. The caudal NM contains morphologically and physiologically distinct cell types (Hong et al., 2018; X. Wang, Hong, Brown, Sanchez, & Wang, 2017), and thus was excluded from the analysis to avoid potential cell type-specific changes. For each section, images were taken from both NMs with a ×20 objective lens attached on an Olympus FV-1200 confocal microscope at a resolution of 0.175 μm per pixel. Images from the same animal were captured with the same imaging parameters. We then followed the intensity analyzing protocol described in a previous study (McBride et al., 2013). Briefly, in each NM, neurons with an identifiable boundary and a well-defined nucleus were selected based on NeuroTrace staining. For each selected neuron, the optical density (OD) of FMRP was measured as the mean gray value of the somatic FMRP immunostaining with background subtraction in Fiji software (National Institutes of Health). For each section, the mean and *SD* of ODs of all measured neurons from the left NM (mean $OD_{left\ NM}$ and *SD* of $OD_{left\ NM}$) were used as standards to which the OD of each neuron in the left and right NMs was normalized as a z-score, where z-score = ($OD_{individual}$ -mean $OD_{left\ NM}$)/*SD* of $OD_{left\ NM}$. The z-score of a particular neuron thus indicates the number of standard deviations that a neuron's OD is away from the mean OD of collective neurons in the left NM within the same section.

Z-scores of all measured neurons from all animals within the same experimental group were pooled for each NM to generate a grouped z-score frequency histogram. In addition, z-scores were compared between the two NMs in each experimental group using Student's paired *t*-test, and between experimental groups and the control group using Student's unpaired *t*-test. For these comparisons, the mean z-score of each NM in each animal was used as a data point. Statistical analyses were performed using GraphPad Prism 6 (GraphPad, San Diego, CA). Significance was determined by $p < .05$. Data were given as mean ± *SD*.

2.8 | Quantification of Y10B intensity and correlation with FMRP

Five animals at 1–2 weeks following a removal of the right cochlea were used for this analysis. For each animal, two sections containing the intermediate and rostral NM were triple labeled with FMRP, Y10B, and NeuroTrace. The same procedure described in *Quantification of changes in FMRP intensity* was used for Confocal image acquisition as well as neurons selection for analyses. For each selected neuron, the intensities of Y10B and FMRP immunostaining within the cell body were measured as the mean gray value of the somatic Y10B and FMRP immunostaining with background subtraction, respectively. Normalization of Y10B and FMRP intensities of each neuron were processed relative to the mean Y10B and FMRP intensities of all measured neurons in the intact NM, respectively. The intensity of each neuron represented an individual data point for statistical analyses. Pearson's correlation analysis was performed between the normalized Y10B and FMRP intensities at the individual cell level using Prism software.

2.9 | Quantification of cell size and correlation with FMRP

Four animals at 1–2 weeks following a removal of the right cochlea were used for this analysis. For each animal, two to three sections containing the intermediate and rostral NM were triple labeled with FMRP, gephyrin, and NeuroTrace. Confocal image stacks were captured with a ×60 oil-immersion lens with a Z interval of 0.5 μm. Neurons with an identifiable boundary and a well-defined nucleus were selected based on NeuroTrace staining at one representative focal plane, and their cell sizes were evaluated by measuring the cross section cell body areas. The intensity of FMRP in each neuron was measured and normalized using the same procedure described in *Quantification of Y10B intensity and correlation with FMRP*. Pearson's correlation analysis was performed between the cell size and normalized FMRP intensity at the individual cell level using Prism software.

2.10 | Quantification of SNAP25 coverage and correlation with FMRP

Four animals at 1–2 weeks following a removal of the right cochlea were used for this analysis. For each animal, two to three sections containing the intermediate and rostral NM were triple labeled with FMRP, SNAP25, and NeuroTrace. The same procedure described in *Quantification of cell size and correlation with FMRP* was used for Confocal image stacks acquisition. Neurons with the entire cell body contained within the same image stack were selected. For a balanced sampling across animals, 15–25 neurons were selected from each side of each animal. For each selected neuron, three representative focal planes with a well-defined cell body boundary and a well-defined nucleus based on NeuroTrace staining were used for the following analyses. To quantify SNAP25-labeled synaptic structures, a threshold was set to enhance the signal-to-noise ratio of SNAP25 staining in the Fiji software. This threshold was fixed for all images from the same animal. The length of SNAP25-labeled structures surrounding the soma was then measured at each focal plane. The somatic coverage of SNAP25-labeled presynaptic structures was calculated as the sum of the length of the SNAP25-labeled structure divided by the somatic perimeter. For each neuron, the mean coverage was averaged from three focal planes, representing a data point. To measure FMRP intensity, the OD of FMRP immunostaining was measured at one of the representative focal planes containing a well-defined nucleus. Following background subtraction, FMRP intensity of each neuron was normalized to the mean FMRP intensity of all measured neurons in the intact NM. Pearson's correlation analysis was performed between the normalized FMRP intensity and the SNAP25 somatic coverage at the individual cell level using Prism software.

2.11 | Quantification of gephyrin intensity and correlation with FMRP

The animals and sections selected for cell size analysis were used here. The same procedure described in *Quantification of SNAP25 coverage and correlation with FMRP* was used for neurons and focal planes selection, and measurement of FMRP intensity for this analysis. For each selected neuron, a region of interest (ROI) was defined by the smallest area along the cell membrane that contained distinct gephyrin immunostaining. The OD of gephyrin immunostaining within this ROI was measured and averaged across three focal planes. The resultant mean intensity represented the gephyrin intensity of the neuron. Normalization of gephyrin and FMRP intensities of each neuron were processed relative to the mean gephyrin and FMRP intensities of all measured neurons in the intact NM, respectively. Pearson's correlation analysis was performed between the normalized FMRP and gephyrin intensities at the individual cell level using Prism software.

2.12 | Illustration

Image brightness, contrast, and gamma were adjusted using Adobe Photoshop (Adobe System, Mountain View, CA) for the purpose of illustration. Figure graphing was performed in Adobe Photoshop and Illustrator (Adobe System). Histogram and statistical graphing were performed in GraphPad Prism.

3 | RESULTS

3.1 | Generation and validation of FMRP antibodies

To examine the expression of endogenous FMRP, we generated a polyclonal antibody (PA8263) that recognizes chicken FMRP. The

immunogen was a synthetic peptide corresponding to amino acid 484–503 (corresponding to 551–570 of human protein) near the C-terminus of the chicken full length protein and conjugated to keyhole limpet hemocyanin protein. To test antibody specificity, western blot was performed on homogenized brainstem tissue samples from P4 chickens. A single band at the expected molecular weight of the chicken FMRP (~70 KDa) was detected (Figure 1a) (Price, Zhang, Ashley Jr., & Warren, 1996; Y. Wang et al., 2014). This band was persistent with and without phosphatase treatment (Figure 1b, right), indicating its recognition of both phosphorylated and unphosphorylated proteins. In contrast, a phospho-specific (Ser499) FMRP antibody (p-FMRP; P1125) recognized chicken proteins of a similar molecular weight as PA8263 in untreated samples, but not in samples treated with phosphatase (Figure 1b, left). Finally, we confirmed antibody specificity to FMRP using a genetic approach. FMRP expression in a subset of NM neurons was knocked down by introducing a specific shRNA via *in ovo* electroporation (X. Wang et al., 2018). Transfected (EGFP+) cells exhibited little PA8263 immunoreactivity (Figure 1c,d; dashed lines), compared to neighboring non-transfected cells which were strongly FMRP immunoreactive (Figure 1c,d; solid lines). Together, we show that PA8263 and P1125 are specific antibodies for FMRP and phosphorylated FMRP, respectively, in the chicken brain.

3.2 | Normal FMRP expression: Cell-to-cell variation and left-to-right symmetry

Using PA8263 antibody, we examined the pattern of FMRP distribution in normally innervated NM of control animals, focusing on the rostral two-thirds of the nucleus, which contains a homogenous neuronal cell type (Hong et al., 2018; X. Wang et al., 2017). We found that most, if not all, NM neurons showed distinct somatic FMRP immunostaining (Figure 2a–c), consistent with our previous observation using a different antibody (Y. Wang et al., 2014). To assess the variation of FMRP intensity across neurons, we calculated the z-score of FMRP immunostaining as the number of standard deviations that a

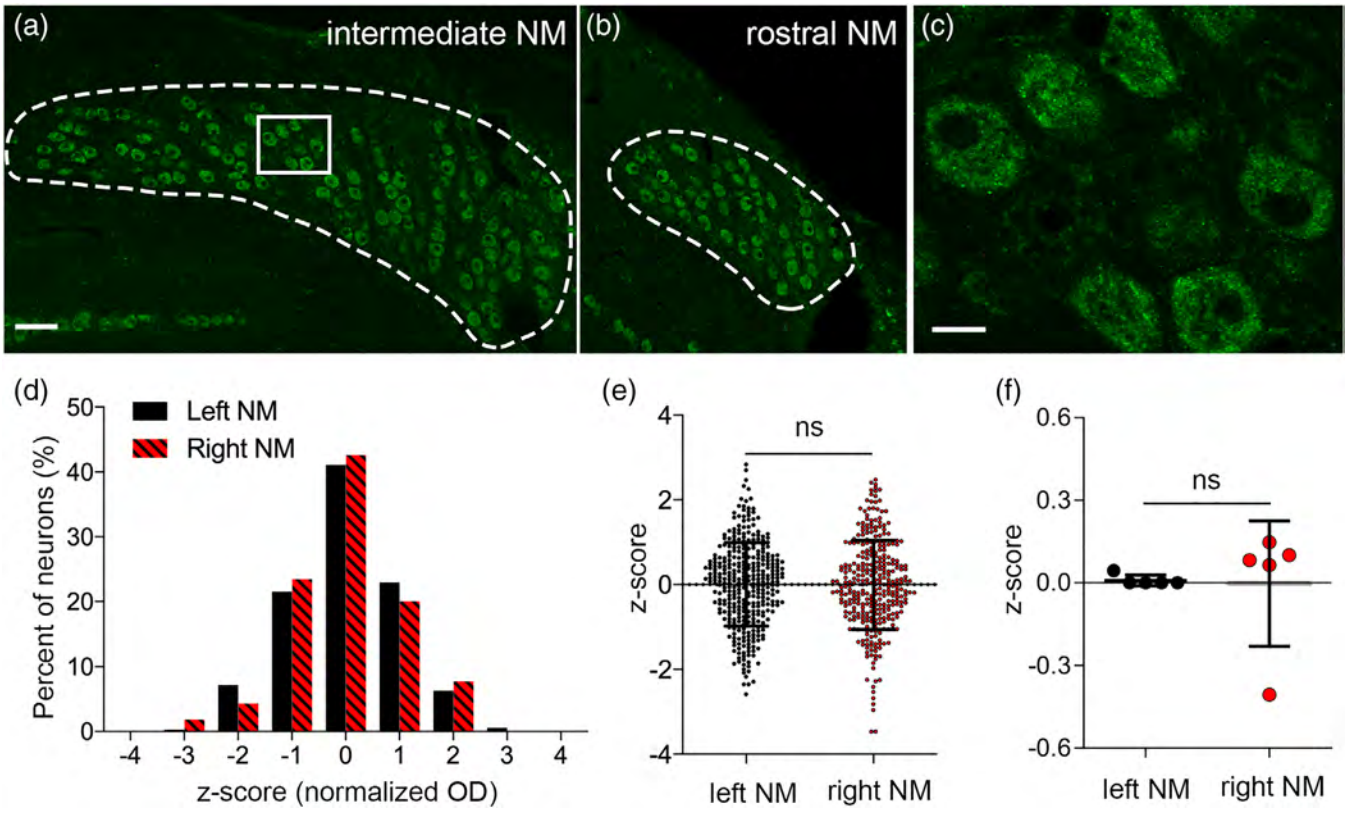

FIGURE 2 Normal FMRP immunoreactivity in NM neurons. (a, b) Representative coronal sections of intermediate (a) and rostral (b) NM, respectively. Dashed lines outline the border of the NM. (c) High-magnification view of the box in (a). (d) Frequency histograms of z-scores of FMRP immunostaining in the left and right NMs. Z-score was used to normalize FMRP OD of each NM neuron to the mean FMRP OD of all neurons in the left NM. The distribution pattern of z-scores is comparable between the left and right NMs in control animals. Each neuron represents an individual data point in the frequency histogram. (e,f) Comparisons of z-scores between the left and right NMs with each neuron (e) and each animal (f) as an individual data point, respectively. Neither analysis revealed a significant difference in z-scores between the left and right NMs. NM, nucleus magnocellularis; OD, optical density; ns, no significance. Scale bars = 50 μm in a (applies to a-b); 10 μm in c [Color figure can be viewed at wileyonlinelibrary.com]

neuron's OD is from the mean OD of all neurons in the left NM within the same section. Across all neurons analyzed from five animals (n = 348 from left NM; n = 328 from right NM), FMRP z-scores exhibited a normal distribution in both the left and right NMs, confirmed by Anderson-Darling and Kolmogorov–Smirnov tests (Figure 2d). The majority of the neurons (> 98%) had a z-score ranging from −2 to 2. More than 85% of neurons had a z-score within −1 to 1, demonstrating a high uniformity of FMRP expression levels among NM neurons under the control condition. Between the left and right NMs, there was no significant difference in z-score at either the individual cell (left: 0.008 ± 0.053, n = 348 neurons; right: 0.007 ± 0.058, n = 328 neurons; p = .846, Student's unpaired t-test; Figure 2e) or animal level (left: 0.009 ± 0.020; right: −0.002 ± 0.227; n = 5 animals; p = .919, Student's paired t-test; Figure 2f). This symmetric distribution validates the use of the left NM as an intra-animal and intra-section control for assessing changes in FMRP immunoreactivity in the right NM following afferent deprivation.

3.3 | Afferent deprivation results in rapid FMRP aggregation into puncta

Previous studies have showed that sensory stimulation leads to increased FMRP levels in cortical neurons within minutes to hours (Gabel et al., 2004; Todd & Mack, 2000; Weiler et al., 1997). Here, we examined whether afferent deprivation triggers rapid FMRP changes in NM neurons. The right cochlea was removed from chicken hatchlings; the NM region was examined at 2, 4, and 6 hr after surgery (n = 5 animals for each group). During this period, there is no cell loss. For the purpose of description, the right and left NMs are named afferent-deprived and intact NMs, respectively. Unoperated animals that did not undergo cochlea removal are control animals.

As compared to the intact NM from the same animal (Figure 3a), the pattern of FMRP immunostaining in the afferent-deprived NM changed dramatically (Figure 3b–d). In a subset of cell bodies, FMRP immunoreactivity aggregated into bright puncta as early as 2 hr

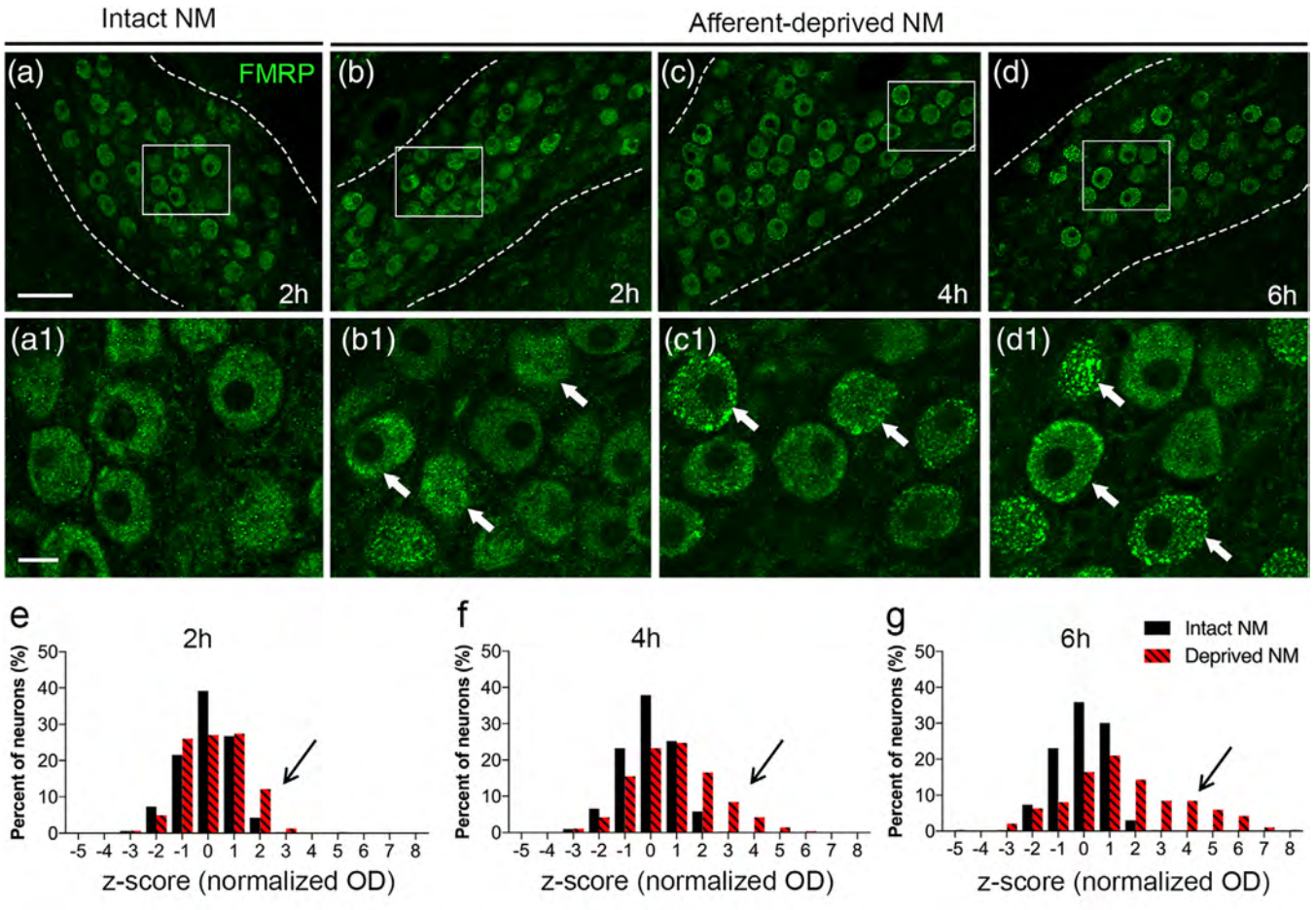

FIGURE 3 Time course of FMRP immunoreactivity changes in NM neurons at 2–6 hr following unilateral cochlea removal. (a–d) Representative images showing FMRP immunoreactivity in the intact (a) and afferent-deprived NMs at 2, 4, and 6 hr (b–d), respectively. Dashed lines outline the border of NM. (a1–d1) High-magnification views of the boxes in (a–d), respectively. Arrows point to neurons exhibiting distinct FMRP puncta in the afferent-deprived NM. (e–g) Frequency histograms of z-scores of FMRP immunoreactivity in the intact and afferent-deprived NMs. Arrows in (e–g) point to a shift of z-scores toward the positive direction. h, hour; NM, nucleus magnocellularis; OD, optical density. Scale bars = 50 μm in a (applies to a–d); 10 μm in a1 (applies to a1–d1) [Color figure can be viewed at wileyonlinelibrary.com]

(arrows in Figure 3b1). This phenotype became more dramatic at 4–6 hr (arrows in Figure 3c1, 3d1), so that about half (48.8%, 139 in 285 neurons) of the neurons in the deprived NM showed a clear punctate pattern at 6 hr. These puncta were distributed throughout the cytoplasm and sometimes near the plasma membrane. In contrast, the remaining neurons in the afferent-deprived NM and all neurons in the intact NM exhibited a normal granular pattern of FMRP labeling. To exclude the possibility that this punctate pattern was caused by nonspecific autofluorescence changes, we performed peroxidase staining of FMRP immunoreactivity (Figure 4a–d). Consistently, FMRP aggregation was evident in a subset of afferent-deprived NM neurons (arrows in Figure 4d), while the remaining neurons (arrowheads) maintained the control pattern. Moreover, we detected a similar aggregation of p-FMRP in the afferent-deprived NM (Figure 4f), in contrast to the uniform staining of p-FMRP in the intact NM (Figure 4e). Collectively, these results demonstrate a rapid formation of FMRP puncta following afferent deprivation, and these puncta contain the phosphorylated form of FMRP.

Quantification analyses revealed that the intensity of FMRP immunoreactivity per cell body was increased following afferent deprivation. The z-score histogram of the afferent-deprived NM shifted toward the positive side relative to the intact NM over time (arrows in Figure 3e–g). The percentage of neurons with a z-score above 2 was significantly increased at 4 and 6 hr in the afferent-deprived NM compared to the right NM of the control animals (control: 2.6 ± 2.0%, n = 5 animals; 4 hr: 23.0 ± 14.6%, n = 5 animals, p = .034; 6 hr: 38.7 ± 8.8%, n = 5 animals, p = .0005; Student's unpaired t-test; Figure 5a, Table 1). Consistently, the mean z-scores across all measured neurons from the afferent-deprived NM at 4 and 6 hr were significantly higher than that of control animals(control: −0.002 ± 0.227; n = 5 animals; 4 hr: 0.863 ± 0.482, n = 5 animals, p = .012; 6 hr: 1.797 ± 0.488, n = 5 animals, p = .0004; Figure 5c).

We next examined the relationship between neurons showing FMRP aggregation and neurons with a high z-score of FMRP intensity (Figure 6a, Table 2). At 6 hr following cochlea removal, more than half (60.4%, 84 in 139 neurons) of the neurons with FMRP aggregation had a z-score above 2. The mean z-score of FMRP-aggregated neurons was significantly higher than that of neurons from the intact NM (intact NM: 0.000 ± 0.986, n = 329 neurons; afferent-deprived NM with FMRP aggregation: 3.112 ± 2.803, n = 139 neurons; p < .0001). Similarly, most of the neurons (77.8%, 84 in 108 neurons) with a z-

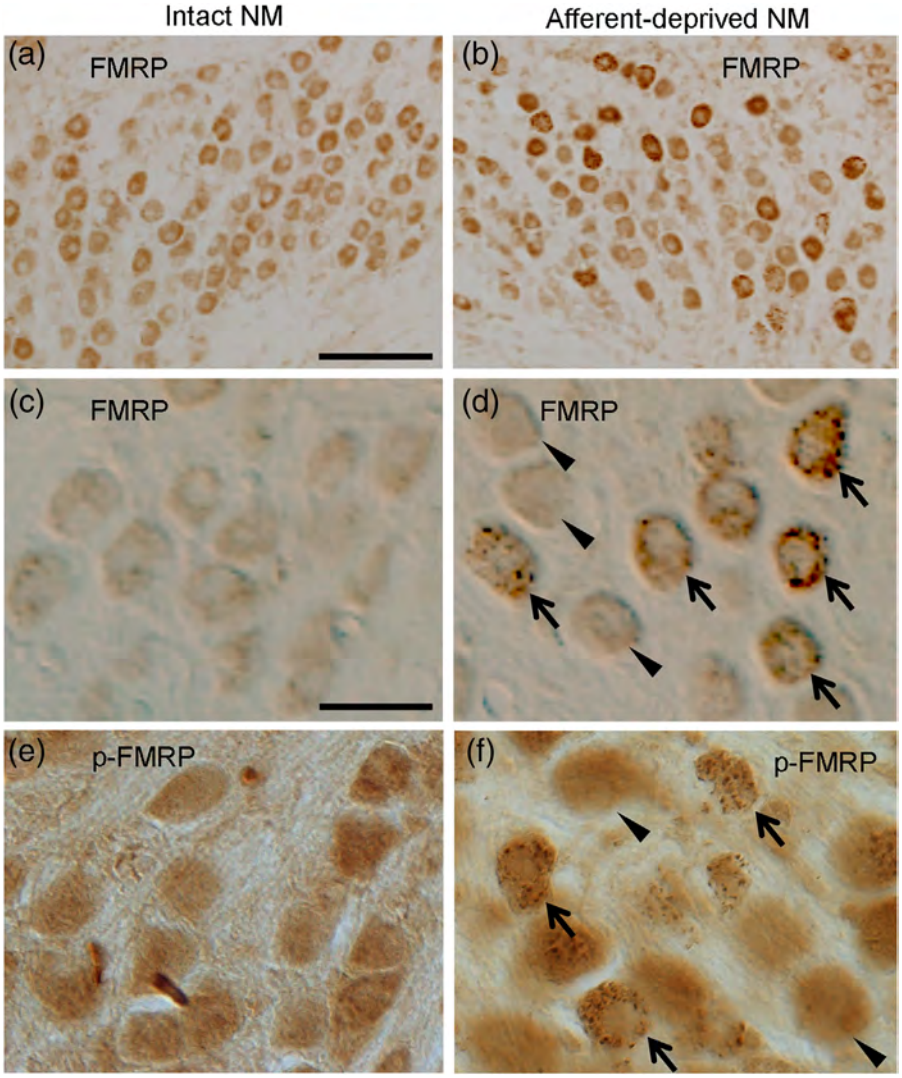

FIGURE 4 Peroxidase staining of FMRP and p-FMRP immunoreactivities at 6 hr following unilateral cochlea removal. (a, b) Bright-field images showing FMRP immunoreactivity in the intact (a) and afferent-deprived (b) NMs. A subset of NM neurons in (b) show stronger FMRP staining. (c, d) Higher-magnification differential interference contrast (DIC) images of FMRP immunoreactivity in the intact (c) and afferent-deprived (d) NMs. Arrows and arrowheads point to neurons with and without FMRP puncta, respectively, in the afferent-deprived NM. (e, f) DIC images of p-FMRP immunoreactivity in the intact (e) and afferent-deprived (f) NMs. Arrows and arrowheads point to neurons with and without p-FMRP puncta, respectively, in the afferent-deprived NM. NM, nucleus magnocellularis. Scale bars = 100 μm in a (applies to a, b); 20 μm in c (applies to c–f) [Color figure can be viewed at wileyonlinelibrary.com]

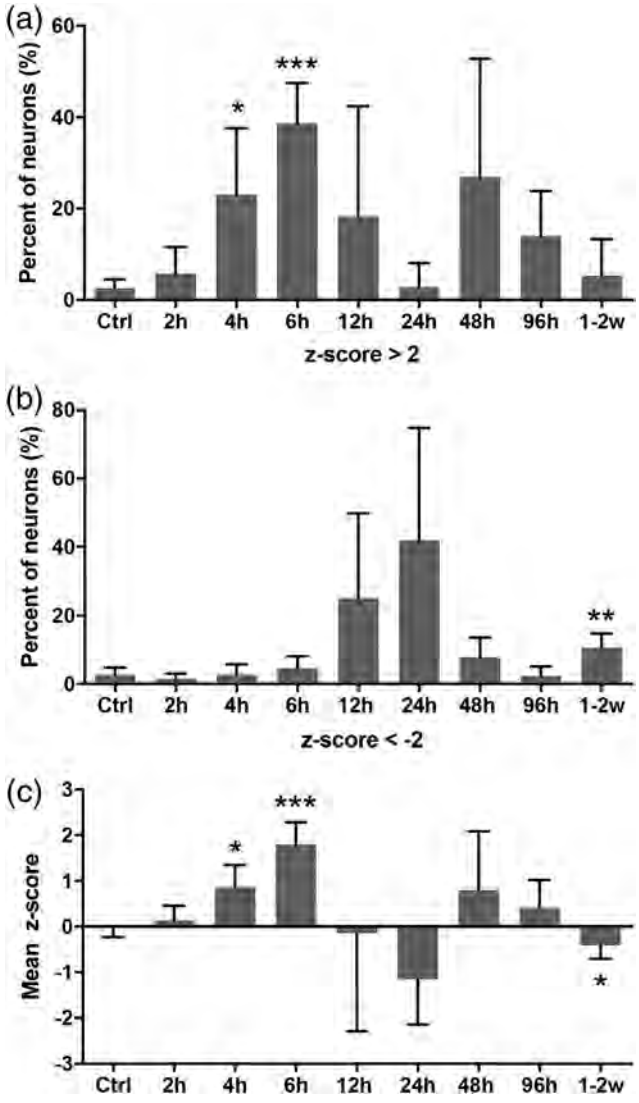

FIGURE 5 Changes in FMRP immunoreactivity in afferent-deprived NM at the population level. (a, b) Percentages of neurons with z-scores above 2 (a) or below −2 (b) in the control (ctrl) and afferent-deprived NMs. (c) Mean z-scores of FMRP immunoreactivity in the control and afferent-deprived NM. Each animal represents an individual data point in these analyses. The significant difference between each experimental group and the control group was determined by Student's unpaired *t*-test with Welch's correction. Exact *p* values are listed in Table 1. ***$p < .001$, **$p < .01$, *$p < .05$. ctrl, control; h, hour; w, week [Color figure can be viewed at wileyonlinelibrary.com]

score above 2 at 6 hr exhibited FMRP aggregation. These results indicate that neurons that have undergone FMRP aggregation are a major contributor of the observed increase in FMRP immunoreactivity in the afferent-deprived NM.

3.4 | FMRP changes are associated with cell fate following afferent deprivation

Persistent afferent deprivation beyond the first 6–8 hr leads to cell death in a subset of NM neurons (Born & Rubel, 1985, 1988). Rapid and differential changes of FMRP in afferent-deprived NM neurons give rise to the possibility that FMRP dynamics may be associated with cell fate determination. We examined this possibility by characterizing the time course of FMRP at 12–24 hr following the removal of the right cochlea. During this time window, dying neurons are recognizable with condensed nuclei and reduced cytoplasm staining by Nissl stain (Born & Rubel, 1985; McBride et al., 2013; Steward & Rubel, 1985).

At 12–24 hr following cochlea removal, three groups of neurons were detected in the afferent-deprived NM based on the following qualitative and quantitative criteria (Figure 7b-b2, 7c-c2). Group 3 was defined as neurons with visually-identifiable FMRP puncta via blind analysis of two individuals. The remaining neurons were assigned to Groups 1 and 2 depending on the value of z-score: Group 1 (above −2) and Group 2 (below −2). At 12 hr, Group 1 exhibited normal Nissl stain and unchanged FMRP distribution and intensity (stars in Figure b1–b2, c1–c2), comparable to the neurons in the intact NM of the same animals (Figure 7a–a2). These neurons represented 51.8% of all measured neurons (117 in 226 neurons) in the afferent-deprived NM. Group 2 had notably lower levels of FMRP immunostaining and no distinct FMRP puncta, representing 26.1% of all neurons (59 in 226 neurons; arrowheads in Figure 7c2). These neurons exhibited a normal Nissl stain, indicating their survival. Group 3 represented 22.1% of all neurons (50 in 226 neurons), characterized by abnormal Nissl stain and distinct FMRP puncta (arrows in Figure 7b1–b2, c1–c2). As compared to earlier time points (2–6 hr), FMRP puncta were larger in size and less in number per cell body and distributed closely to the plasma membrane. At 12 hr, these cells had a condensed nucleus stain with dramatically reduced cytoplasmic Nissl substance (arrows in Fig. 7b2). By 24 hr, many of these cells had lost cytoplasmic Nissl

TABLE 1 Statistical significance (*p* value) comparing z-scores of FMRP immunoreactivity between experimental and control groups

	2 hr	4 hr	6 hr	12 hr	24 hr	48 hr	96 hr	1–2 week
z-score > 2	0.284	0.034 (*)	0.0005 (***)	0.219	0.921	0.156	0.100	0.485
z-score < −2	0.338	0.989	0.350	0.111	0.056	0.169	0.836	0.009 (**)
Mean z-score	0.454	0.012 (*)	0.0004 (***)	0.891	0.057	0.302	0.270	0.040 (*)

Note: Each animal represents an individual data point. Significant difference between each experimental group and the control group was determined by Student's unpaired *t*-test with Welch's correction.

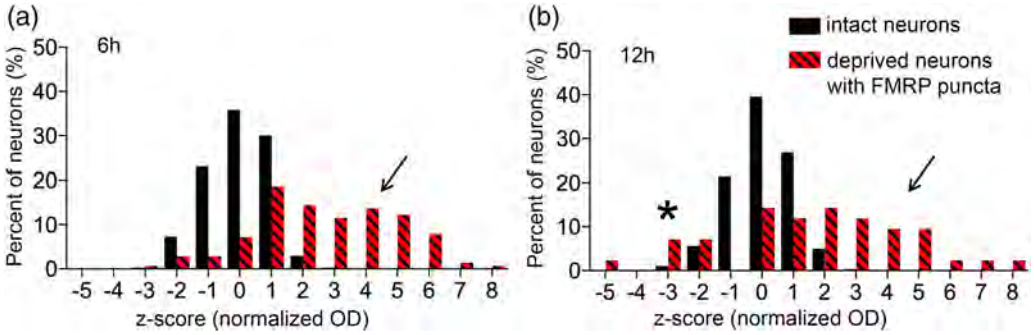

FIGURE 6 Frequency histograms of FMRP z-scores in afferent-deprived NM neurons with FMRP puncta. (a, b) show analyses from 6 and 12 hr, respectively. Intact neurons are all neurons in the left NM of the same animals. Arrows and star point to the population with high and low z-scores, respectively. h, hour; OD, optical density [Color figure can be viewed at wileyonlinelibrary.com]

z-score	Control	2 hr	4 hr	6 hr	12 hr	24 hr	48 hr	96 hr	1–2 week
> 2	2.6	5.8	23.0	38.7	18.3	2.8	26.9	14.0	5.3
< –2	2.7	1.5	2.7	4.5	25.1	41.9	7.9	2.3	10.6

Note: The data were pooled across all animals in each control and manipulated group.

TABLE 2 Percentages (%) of neurons with z-scores above 2 or below –2

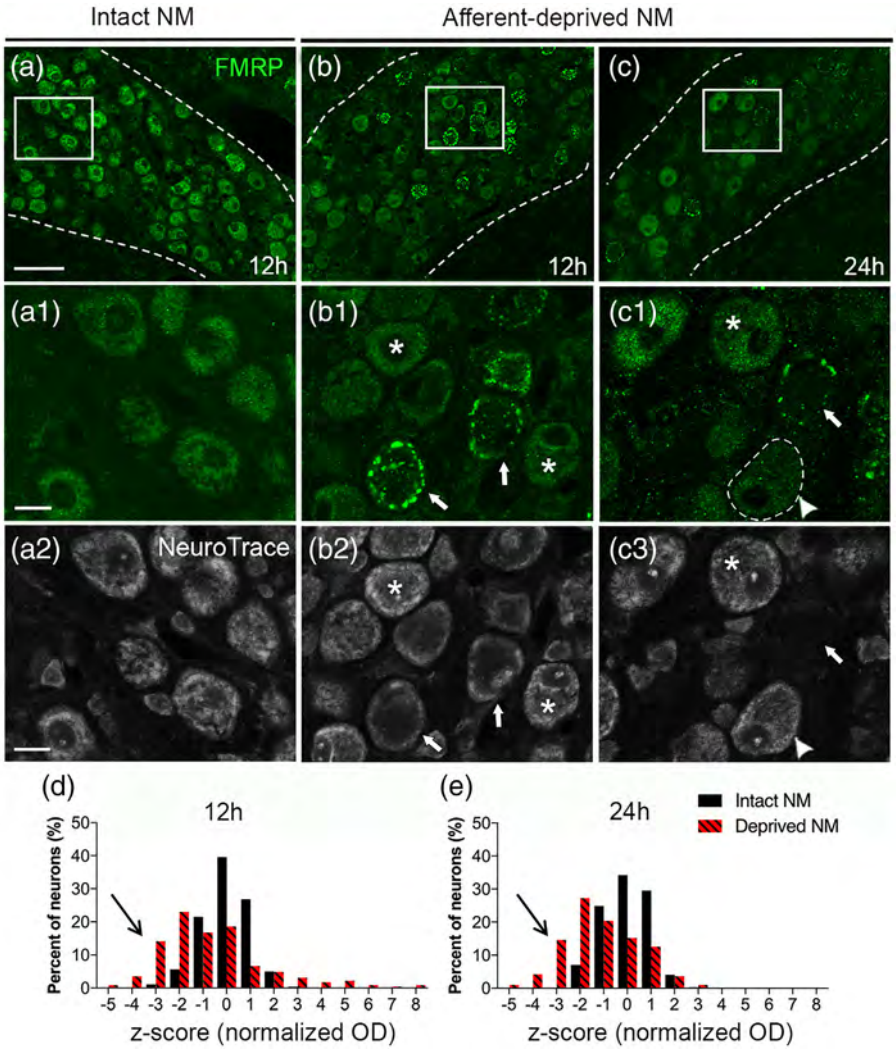

FIGURE 7 Time course of FMRP immunoreactivity changes in NM neurons at 12 and 24 hr following unilateral cochlea removal. (a–c) Representative images showing FMRP immunoreactivity in the intact (a) and afferent-deprived NMs at 12 (b) and 24 hr (c). Dashed lines outline the border of the NM. (a1–c1) High-magnification view of the boxes in (a–c), respectively. (a2–c2) NeuroTrace staining of the same regions in (a1–c1). Stars indicate neurons with normal looking Nissl and FMRP staining. Arrows point to neurons exhibiting distinct FMRP puncta and reduced cytoplasmic Nissl substance. Arrowheads indicate neurons with normal Nissl stain but low FMRP immunostaining (dashed circle). (d, e) Frequency histograms of z-scores of FMRP immunoreactivity in the intact and afferent-deprived NM neurons. h, hour; NM, nucleus magnocellularis; OD, optical density. Scale bars = 50 μm in a (applies to a–c); 10 μm in a1 (applies to a1–c2) [Color figure can be viewed at wileyonlinelibrary.com]

substance almost completely, leaving an empty space on Nissl stain (arrow in Figure 7c2). A few residual FMRP puncta were still present (arrow in Figure 7c1), indicating cell membrane integrity at this time.

Quantification of z-scores confirmed the presence of neurons with low FMRP intensities in the afferent-deprived NM. The z-score histogram of the afferent-deprived NM shifted toward the negative side relative to the intact NM at 12–24 hr (arrows in Figure 7d,e). However, there is no significant increase of the percentage of neurons with z-score < −2 at 12 hr (25.1 ± 24.6%, n = 5 animals, p = .111) and 24 hr (41.9 ± 32.9%, n = 5 animals, p = .056) compared to the right NM of the controls (2.7 ± 2.1%, n = 5 animals; Student's unpaired t-test; Figure 5b, Table 1). Similar to 6 hr, half of (25 in 50 neurons) the neurons that exhibit FMRP puncta (Group 3) continued to have a high z-score (above 2) at 12 hr (arrow in Figure 6b). A small percentage of neurons in Group 3 (12%, 6 in 50 neurons; star in Figure 6b) with a very low z-score (below −2) may reflect neurons undergoing degradation at 12 hr. At 24 hr, as the "ghost" neurons without a well-defined cell body boundary in Nissl stain were not included in the analysis, neurons with low z-scores (below −2) mostly belonged to Group 2.

Together, neurons with abnormal Nissl stain, which predicts cell death, at 12–24 hr following afferent deprivation show distinct and persistent FMRP puncta (Group 3). Surviving neurons, as indicated by a normal pattern of Nissl stain, do not show FMRP puncta, although their FMRP intensity varies (Groups 1 and 2).

3.5 | Prolonged afferent deprivation leads to FMRP fluctuation in surviving neurons

All neuronal cell death in NM occurs within 2 days following unilateral cochlea removal (Born & Rubel, 1985). We next examined FMRP dynamics in surviving NM neurons at 2–4 days following afferent deprivation. This time period represents a transition window during which the system regains its homeostasis after surgery. During this period, the intracellular FMRP staining pattern was largely comparable between the intact and

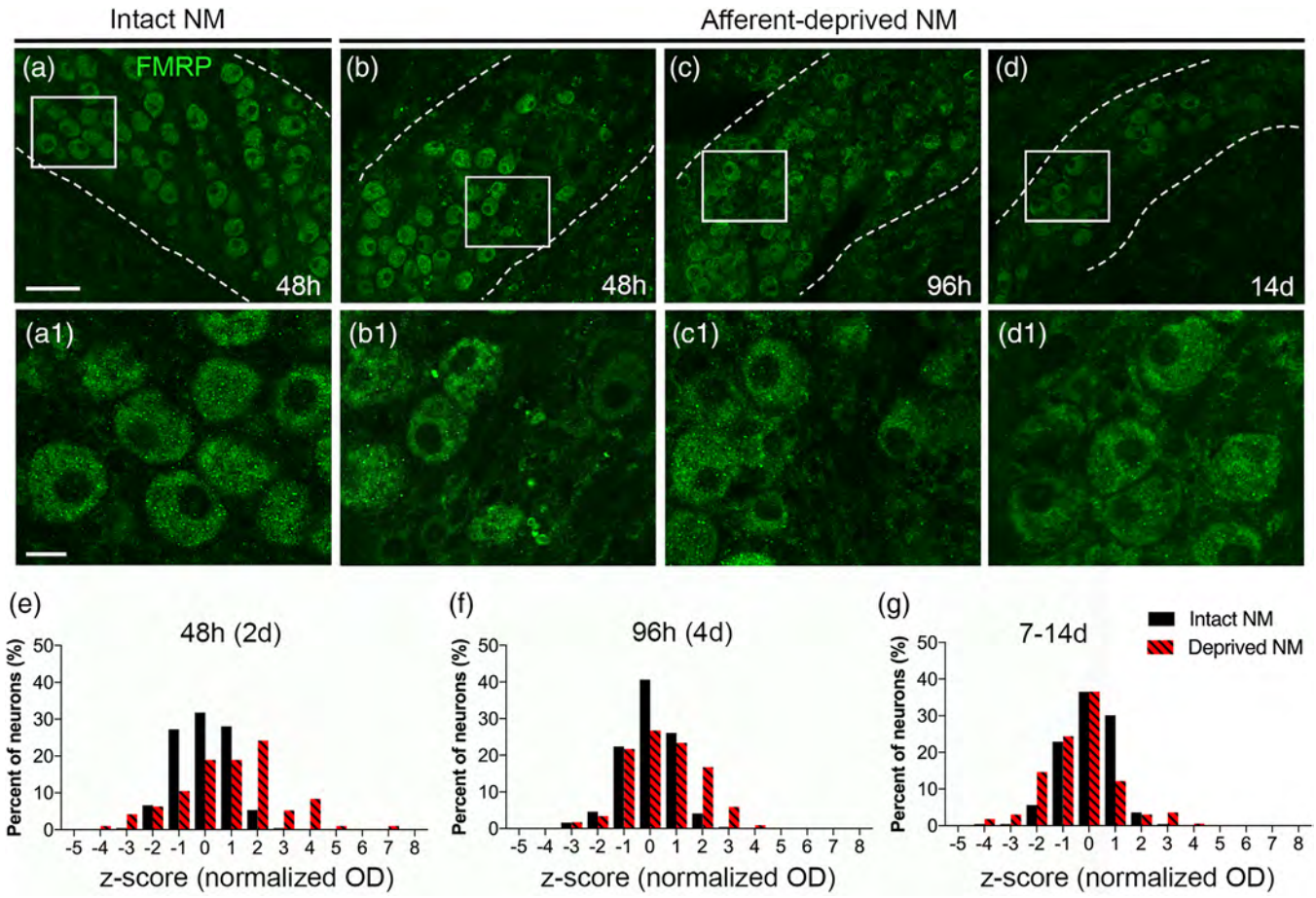

FIGURE 8 Time course of FMRP immunoreactivity changes in NM neurons from 48 hr to 2 weeks following unilateral cochlea removal. (a–d) Representative images showing FMRP immunoreactivity in the intact (a) and afferent-deprived NMs at 48 hr (b), 96 hr (c), and 1–2 weeks/7–14 days (d). Dashed lines outline the border of the NM. (a1-d1) High-magnification view of the boxes in (a–d), respectively. (e–g) Frequency histograms of z-scores of FMRP immunoreactivity in the intact and afferent-deprived NM neurons. d, day; h, hour; NM, nucleus magnocellularis; OD, optical density. Scale bars = 50 μm in a (applies to a-c); 10 μm in a1 (applies to a1–d1) [Color figure can be viewed at wileyonlinelibrary.com]

afferent-deprived NM, with comparable z-scores (Figures 5c, 8a–c, Table 1). However, compared to the intact NM (Figure 8a1), the afferent-deprived NM showed increased heterogeneity in FMRP intensity (Figure 8b1–c1) which is consistent with a more dispersed distribution of z-scores (Figure 8e-f). A substantial number of neurons had a z-score beyond the −2 to 2 range at 48 hr (34.8%) and 96 hr (16.3%), compared to only 5.2% in control animals (Table 2).

Next, we examined the homeostatic FMRP expression at 1–2 weeks following cochlea removal. FMRP immunoreactivity exhibited a granular pattern (Figure 8d–d1), comparable to the control animals. On average, about 16% of neurons in the afferent-deprived NM had a z-score beyond the −2 to 2 range at 1–2 weeks, and the mean of FMRP z-scores is slightly but significantly lower than control animals (control: −0.002 ± 0.227, n = 5 animals; 1–2 weeks: −0.411 ± 0.291, n = 5 animals; p = .040; Figure 5c). Consistently, the percentage of neurons with a z-score below −2 was significantly increased as compared to control animals (control: 2.7 ± 2.1%, n = 5 animals; 1–2 weeks: 10.6 ± 4.2%, n = 5 animals; p = .009, Student's unpaired t-test; Figure 5b). The distribution of FMRP z-scores maintained its normality in the intact NM but not the afferent-deprived NM (Anderson-Darling test: p = .0003; Kolmogorov–Smirnov test: p = .0015). To summarize, afferent-deprived NM neurons regained FMRP expression homeostasis with slightly increased cell-to-cell heterogeneity and an overall reduction in FMRP intensity.

3.6 | Homeostatic FMRP level is associated with cell size and Y10B immunoreactivity in surviving neurons

Afferent deprivation results in long-lasting changes in neuronal function and synaptic connectivity. To identify a potential involvement of FMRP in these changes, we performed correlation analyses of FMRP intensity with cellular properties and synaptic markers at 1–2 weeks following unilateral cochlea removal (n = 7 animals).

As FMRP is a polyribosome-related RNA binding protein (Darnell et al., 2011; Feng et al., 1997; Maurin, Zongaro, & Bardoni, 2014), we first examined the relationship between FMRP and ribosomal activity. Y10B is an rRNA-specific antibody that has been used extensively in the chicken auditory brainstem and mammalian neurons as a marker for active ribosomes and overall protein synthesis (Garden et al., 1994; Garden, Redeker-DeWulf, & Rubel, 1995; Hyson & Rubel, 1995; H. K. Kim, Kim, Kim, & Schuman, 2005; Koenig, Martin, Titmus, & Sotelo-Silveira, 2000; Lerner et al., 1981; McBride

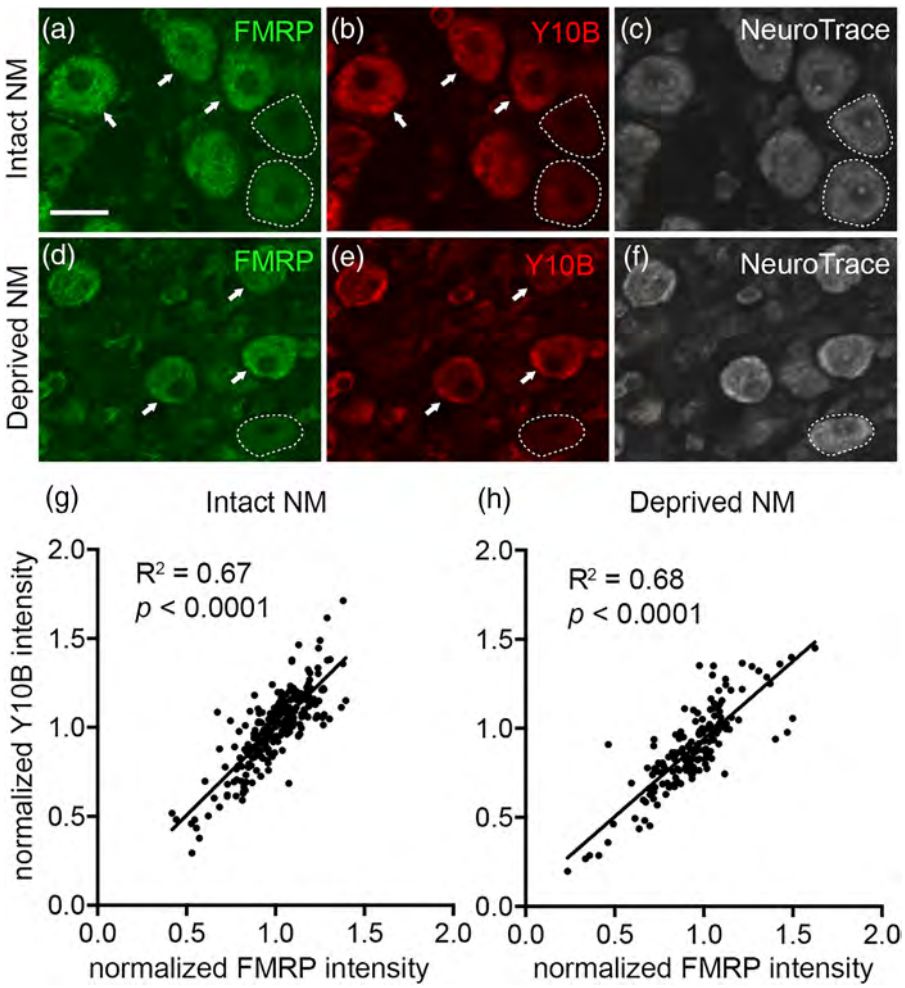

FIGURE 9 Correlation of FMRP intensity with Y10B intensity at 1–2 weeks after unilateral cochlea removal. (a–f) Representative images of triple labeling of FMRP, Y10B, and NeuroTrace in the intact (a–c) and afferent-deprived (d–f) NMs, respectively. Arrows indicate neurons with relatively higher FMRP and Y10B intensities. Dashed lines outline neurons with lower FMRP and Y10B intensities. (g, h) Scatter plots showing correlations between normalized FMRP intensity and normalized Y10B intensity in the intact (g) and afferent-deprived (h) NMs, respectively. NM, nucleus magnocellularis. Scale bar = 15 μm in a (applies to a–f) [Color figure can be viewed at wileyonlinelibrary.com]

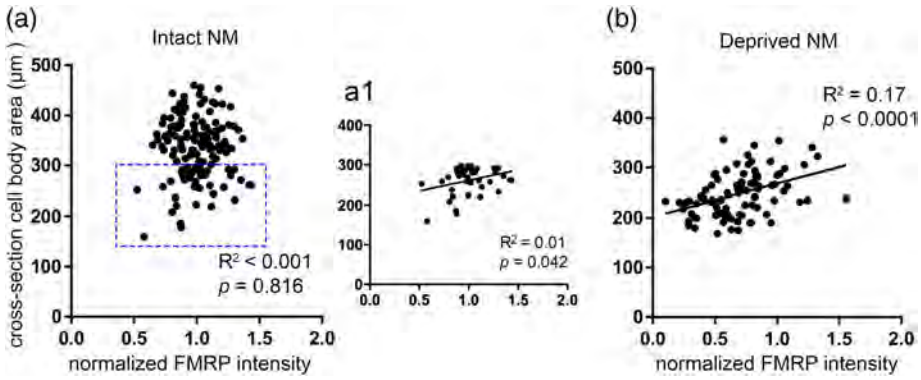

FIGURE 10 Correlation of FMRP intensity with cell body size at 1–2 weeks after unilateral cochlea removal. There is no significant correlation between normal FMRP intensity and cross section cell body area in the intact NM (a). When only including the small cells (less than 300 μm^2), shown in the rectangle in (a) to the correlation analysis, FMRP intensity is moderately correlated with cell size (a1). The correlation is significantly positive in the afferent-deprived NM (b). NM, nucleus magnocellularis [Color figure can be viewed at wileyonlinelibrary.com]

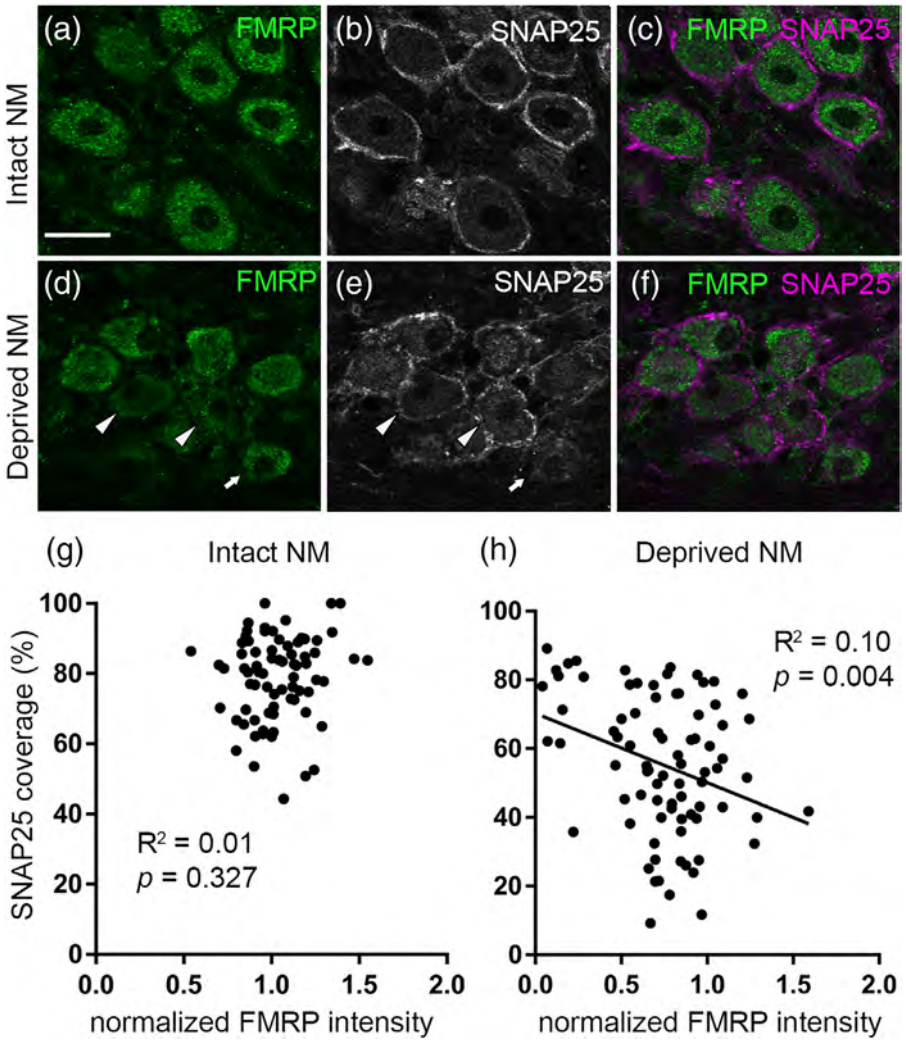

FIGURE 11 Correlation of FMRP intensity with the coverage of SNAP25-positive presynaptic structures at 1–2 weeks after unilateral cochlea removal. (a–f) Representative images of double-labeling of FMRP and SNAP25 in the intact (a–c) and afferent-deprived (d–f) NMs, respectively. Arrows indicate a neuron with relatively higher FMRP but more segmented SNAP25 staining. Arrowheads indicate neurons with relatively lower FMRP but more intact SNAP25 staining. (g, h) Scatter plots showing correlations between normalized FMRP intensity and normalized cell surface coverage of SNAP25-positive presynaptic structures in the intact (g) and afferent-deprived (h) NMs, respectively. NM, nucleus magnocellularis. Scale bar = 30 μm in a (applies to a–f) [Color figure can be viewed at wileyonlinelibrary.com]

et al., 2013). Interestingly, neurons with stronger FMRP immunoreactivity tended to exhibit higher levels of Y10B staining in both the intact NM (Figure 9a–c; arrows vs. dashed circles) and afferent-deprived NM at 1–2 weeks (Figure 9d–f). Indeed, normalized FMRP intensity was highly correlated with normalized Y10B intensity (intact NM: R^2 = 0.67, p < .0001, n = 247 neurons; afferent-deprived NM: R^2 = 0.68, p < .0001, n = 164 neurons; Figure 9g,h). In addition, we detected a significant reduction of normalized Y10B staining in the

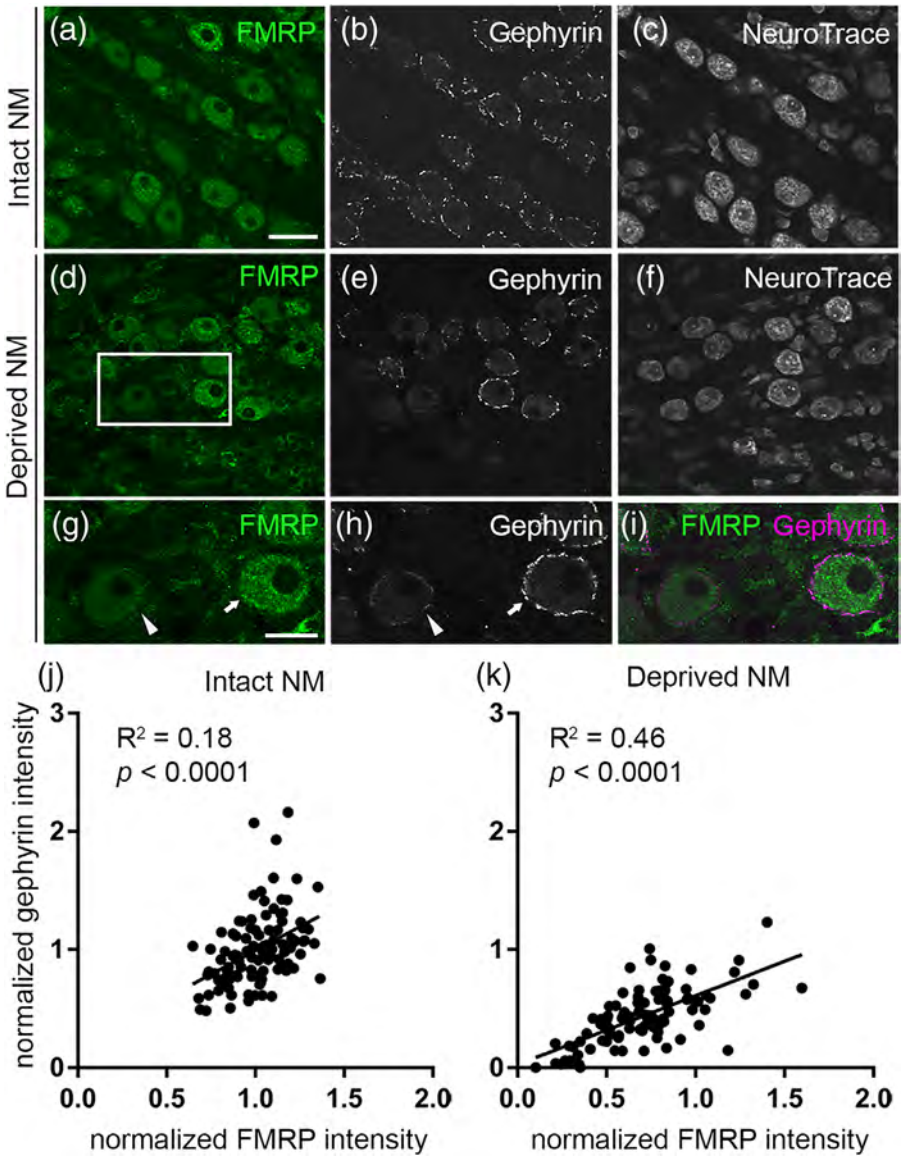

FIGURE 12 Correlation of FMRP intensity with gephyrin intensity at 1–2 weeks after unilateral cochlea removal. (a–f) Representative images of triple labeling of FMRP, gephyrin, and NeuroTrace in the intact (a–c) and afferent-deprived (d–f) NMs, respectively. (g–i) Higher-magnification views of the boxed region in (d). Arrows indicate a neuron with relatively higher FMRP and gephyrin intensities. Arrowheads indicate a neuron with relatively lower FMRP and gephyrin intensities. (j, k) Scatter plots showing correlations between normalized FMRP intensity and normalized gephyrin intensity in the intact (j) and afferent-deprived (k) NMs, respectively. NM, nucleus magnocellularis. Scale bars = 30 μm in a (applies to a–f); 15 μm in g (applies to g–i) [Color figure can be viewed at wileyonlinelibrary.com]

afferent-deprived NM compared to the intact NM (intact NM: 1.00 ± 0.208, n = 247 neurons; afferent-deprived NM: 0.883 ± 0.227, n = 164 neurons, p < .0001, Student's unpaired t-test).

Cochlea removal also leads to a reduction in the cell body size (Born & Rubel, 1985). Therefore, we next examined whether the somatic FMRP level is correlated with the cell body size under normal and afferent-deprived conditions. Based on NeuroTrace staining, we confirmed that cell size, as evaluated by the cross section cell body area, was significantly reduced (26%) in the afferent-deprived NM as compared to the intact NM (intact NM: 335.6 ± 61.5, n = 139 neurons; afferent-deprived NM: 248.2 ± 43.8, n = 88 neurons; p < .0001, Student unpaired t-test). 87.5% (77 in 88 neurons) of afferent-deprived neurons had a cell body area smaller than 300 μm^2. There was no significant correlation between normalized FMRP immunoreactivity and cell body size in the intact NM (R^2 = 0.0004, p = .816; Figure 10a). In contrast, the afferent-deprived NM exhibited a positive correlation of FMRP immunoreactivity with cell size (R^2 = 0.17, p < .0001; Figure 10b). Interestingly, in the intact NM, when we examined only the neurons with a relatively small cell body size (less than 300 μm^2; rectangle in Figure 10a), there was a moderate correlation between FMRP immunoreactivity and the cell body size in this cell population (R^2 = 0.01, p = .042, n = 42 neurons; Figure 10a1).

To summarize, FMRP level is positively correlated with Y10B immunoreactivity regardless of afferent input, and we find a novel correlation of reduced FMRP with reduced cell body size when afferent input is compromised.

3.7 | Homeostatic FMRP level is associated with synaptic distribution in surviving neurons

FMRP regulates synaptic remodeling in an activity-dependent manner (Doll & Broadie, 2015; Doll, Vita, & Broadie, 2017). Therefore, we

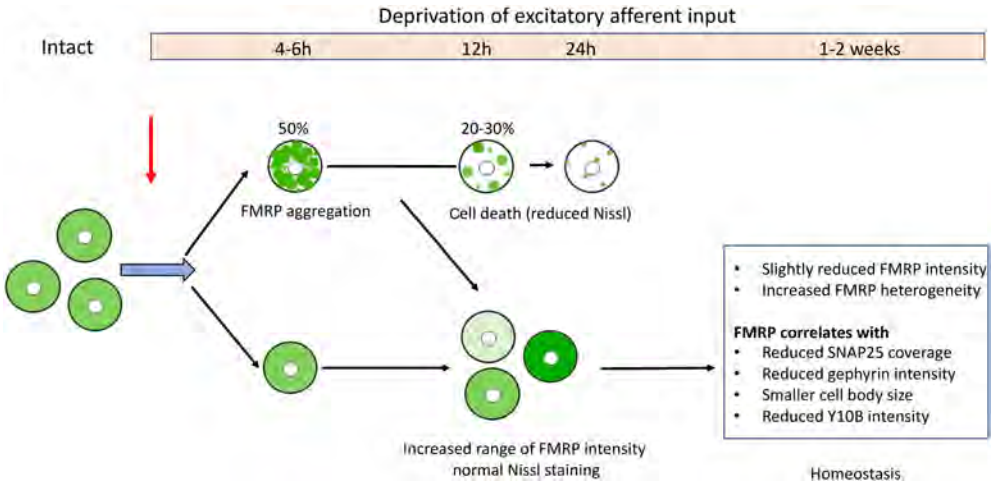

FIGURE 13 Summary of FMRP changes following afferent deprivation. Green color indicates FMRP immunoreactivity in NM neurons. Darker and lighter green indicate higher and lower FMRP intensities, respectively. Red arrow points to the onset of afferent deprivation. Normally innervated NM neurons are relatively uniform in FMRP intensity and cytoplasmic localization. Afferent-deprived NM neurons either maintain a largely normal FMRP pattern or exhibit large FMRP puncta at 2–6 hr. At 12–24 hr, FMRP puncta disappear in some neurons but persist in others. The latter group progresses with cell death as indicated by reduced cytoplasmic Nissl stain. Surviving NM neurons undergo subtle FMRP changes, leading to a small reduction in the mean FMRP level and a small increase in FMRP heterogeneity at 1–2 weeks. The homeostatic FMRP immunoreactivity is associated with cell body size, the overall level of ribosome activity (Y10B), the integrity of presynaptic terminals, and the intensity of inhibitory synaptic protein gephyrin. h, hour [Color figure can be viewed at wileyonlinelibrary.com]

then examined whether afferent deprivation affects the distribution of excitatory and inhibitory synapses on NM neurons and whether these changes are associated with FMRP expression at 1–2 weeks after removal of the right cochlea. As expected, neurons in the intact NM showed distinct and continuous SNAP25, an excitatory presynaptic protein, staining encircling the cell bodies (Figure 11a–c). In the afferent-deprived NM, neurons exhibited a more segmented pattern of perisomatic SNAP25 staining (Figure 11d–f). Moreover, the cell surface covered by SNAP25 was significantly reduced (intact NM: 78.8 ± 12.1%, n = 74 neurons; afferent-deprived NM: 55.4 ± 20.1%, n = 81 neurons; p < .0001, Student's unpaired t-test). There was no significant correlation between FMRP intensity and SNAP25-positive cell surface coverage in the intact NM (R^2 = 0.01, p = .327; Figure 11g). Interestingly, FMRP intensity was negatively correlated with SNAP25 coverage in the afferent-deprived NM (R^2 = 0.10, p = .004; Figure 11h).

Colocalization analyses of FMRP and gephyrin, an inhibitory postsynaptic protein, revealed a significant reduction of gephyrin intensity in afferent-deprived NM neurons. The general pattern of gephyrin localization was comparable between the intact (Figure 12a-c) and afferent-deprived NMs (Figure 12d-i). Normalized gephyrin intensity along the cell plasma membrane was significantly reduced in the afferent-deprived NM as compared to the intact NM (intact NM: 1.00 ± 0.312, n = 103 neurons; afferent-deprived NM: 0.436 ± 0.243, n = 96 neurons; p < .0001, Student unpaired t-test). Correlation analyses revealed a positive correlation of normalized FMRP intensity with normalized gephyrin intensity in both the intact (R^2 = 0.18, p < .0001; Figure 12j) and afferent-deprived NMs (R^2 = 0.46, p < .0001; Figure 12k).

Together, FMRP is associated with postsynaptic gephyrin intensity regardless of afferent input, and exhibits a novel correlation with presynaptic SNAP25-positive structural coverage when afferent input is compromised.

4 | DISCUSSION

Using the primary cochlear neurons in the chicken NM as a model system, this study characterized multi-staged changes in FMRP intensity and subcellular localization following cochlea removal-induced afferent deprivation, as summarized in Figure 13. In addition, we uncovered novel correlations between homeostatic FMRP level and cellular and synaptic properties under both normal and afferent-deprived conditions. The significance of these afferent-regulated FMRP changes is discussed below in terms of its potential involvement in activity-dependent neuronal responses and connectivity reorganization.

4.1 | Potential involvement of FMRP in stress granule and cell survival

One distinct change in FMRP following the deprivation of excitatory afferent input is a rapid aggregation into large puncta within hours. This change is accompanied by a number of other cellular changes, including inhibited phosphorylation of eukaryotic translation elongation factor 2 (McBride et al., 2013), reduced levels of cytoskeletal proteins, tubulin, actin, and microtubule associated protein 2 (Kelley, Lurie, & Rubel, 1997), as well as reduced overall rate of protein

synthesis, metabolic activity, and ribosome integrity (Born et al., 1991; Garden et al., 1994; Garden, Redeker-DeWulf, & Rubel, 1995; Heil & Scheich, 1986; Steward & Rubel, 1985). However, none of these early changes of proteins exhibit subcellular specificity with a punctate pattern. The novel assembly of FMRP into large puncta is reminiscent of cytoplasmic stress granules, the membraneless cytoplasmic assembly of ribonucleoproteins in response to cellular stresses. As an RNA-binding protein, FMRP is indeed a commonly identified component of stress granules in cells treated with heat or oxidative stress (Mazroui et al., 2003; Zalfa, Achsel, & Bagni, 2006) and in the hippocampus after electrode insertion (S. H. Kim, Dong, Weiler, & Greenough, 2006). In addition, phosphorylated FMRP phase separation has been considered a mechanism underlying synaptic activity-dependent neuronal granule formation (Boeynaems et al., 2018; Tsang et al., 2019). Consistently, HeLa cells lacking FMRP exhibit altered stress granule assembly (Didiot, Subramanian, Flatter, Mandel, & Moine, 2009). In addition, FMRP puncta observed in the afferent-deprived NM are similar to typical stress granules in their reversibility. Assembly of FMRP puncta was triggered in about 50% of neurons at 6 hr following afferent deprivation, while on average only about 20% of neurons maintained the FMRP aggregation pattern at 12 hr, implicating a disassembly of FMRP puncta in some NM neurons. To our knowledge, there is no study examining whether stress granules can be induced by afferent deprivation in neuronal systems. Thus, the phosphorylated FMRP puncta that we observed following cochlea removal may indicate a novel formation of stress granules in response to massive afferent deprivation. Interestingly, an in vitro study using an inner-ear-derived cell line reported stress granules following aminoglycoside-induced damage (Towers, Kelly, Sud, Gale, & Dawson, 2011), suggesting that stress granule formation could be a fundamental cellular stress response induced by hearing loss.

Given the protective roles of stress granules in neuronal apoptosis (Buchan & Parker, 2009), one may speculate that FMRP granule assembly in the NM may be involved in afferent-influenced cell survival. Particularly, a protective role of FMRP in non-neuronal cell survival has been reported in response to topoisomerase II inhibitor etoposide treatment (Jeon et al., 2011) and in neuronal apoptosis induced by vascular occlusion (Jeon et al., 2012). Interestingly, our analyses in the afferent-deprived NM demonstrate a link between persistent FMRP aggregation and cell death. The subpopulation of neurons that showed distinct and persistent FMRP puncta were also characterized by reduced cytoplasmic Nissl stain, which indicates that they are dying. On the other hand, surviving neurons, as indicated by normal Nissl stain, did not show FMRP puncta, although they varied in FMRP intensity. There are two possible explanations for this finding which are not mutually exclusive: one is that FMRP aggregates are indeed protective, but unable to rescue dying neurons at the stage when they were captured on imaging; the other is that FMRP aggregates are toxic, causing these neurons to die. The most likely chain of cellular events could be that shortly after cochlea removal, afferent deprivation triggers FMRP-dependent formation of stress granules in NM neurons, which may inhibit protein synthesis and promote cell survival. However, prolonged FMRP aggregation and translational inhibition may eventually lead to cell death, as cells with persistent FMRP aggregation die and only those able to reverse the aggregation survive. In addition, it is important to note that many NM neurons do not exhibit FMRP aggregation and do survive following afferent deprivation, indicating that FMRP assembly/disassembly may not be necessary for cell survival, but persistent FMRP aggregation is linked with cell death once it occurs.

In addition to changes in FMRP localization, the intensity of FMRP immunoreactivity, as evaluated by z-scores, increased, particularly in neurons with notable FMRP aggregation. This increase may be partially attributed to protein aggregation, which often enhances immunostaining intensity without an increase in the amount of proteins, or may be representative of altered FMRP expression. Rapid changes in FMRP expression following afferent manipulations have previously been reported in the barrel and visual corticesshortly after whisker and light stimulation, respectively (Gabel et al., 2004; Todd et al., 2003; Todd & Mack, 2000). However, it is unclear how reduced afferent activity in NM neurons and enhanced afferent activity in cortical neurons result in the same directional change (increase) of FMRP. In the barrel cortex, induced FMRP upregulation requires the activation of metabotropic glutamate receptor (mGluR), as whisker stimulation dependent expression of FMRP was abolished by pharmacological blockade of type I mGluR (Todd et al., 2003). In the NM, removal of mGluR activation increases intracellular calcium concentration and negatively affects ribosome activity, which may eventually contribute to the death of NM neurons (Call & Hyson, 2016; Carzoli & Hyson, 2011; Zirpel & Rubel, 1996). If mGluR activation and inactivation are also involved in afferent-regulated FMRP dynamics in NM, this signal pathway may be a potential candidate for studying differential responses in FMRP expression in response to altered afferent activity across cell types.

4.2 | Potential relationship between FMRP and afferent-regulated cellular properties and synaptic rearrangement

With prolonged afferent deprivation, the FMRP level in surviving NM neurons is further adjusted before it regains homeostasis after 1 week. On average, the intensity of FMRP immunoreactivity in the afferent-deprived NM is slightly but significantly reduced compared to that in the intact NM. Consistently, more neurons show a z-score below the control range. This reduction of FMRP level in afferent-deprived environment is consistent with the observation of increased FMRP in the rat hippocampal dentate gyrus and visual cortex following exposure to enriched environment (Irwin et al., 2000, 2005), demonstrating a positive correlation of FMRP expression with the level of sensory stimulation. On the other hand, there is also a tendency for more neurons exhibiting FMRP intensity above the normal range, indicating a cell-to-cell basis of FMRP dynamics following afferent deprivation.

Our correlation analyses further demonstrate that FMRP level is potentially associated with certain neuronal and synaptic properties depending on the level of afferent inputs. First, afferent deprivation

results in smaller cell bodies. When all neurons were polled for analysis, FMRP level is not associated with cell size in the intact NM but the two properties become positively correlated at 1–2 weeks following afferent deprivation. It is tempting to interpret this as a result of reduced afferent input causing NM neurons with a higher FMRP intensity to have a larger cell body, that is, less cell body shrinkage. In other words, FMRP may be an indicator of healthier neurons that maintain their sizes closer to normal levels. However, a moderate correlation also exists between FMRP and cell size in a small proportion of afferent-intact NM neurons that normally have a smaller cell body (comparable to most neurons following afferent deprivation). This observation of correlated FMRP level and cell size could be interpreted as either: a condition normally seen among small cells that is independent of afferent input but is unmasked by loss of large cells; or the effect of afferent deprivation on FMRP association with cell size. Additionally, a potential methodological artifact that occurs only when the cell body size is small cannot be excluded.

Second, we found that Y10B intensity is reduced following loss of afferent input but maintains a positive association with FMRP intensity in both the intact and afferent-deprived NMs at 1–2 weeks after cochlea removal. If Y10B is a reliable indicator of active protein translation under homeostatic conditions as proposed during the first 12 hr after afferent deprivation (Garden et al., 1994), the observed Y10B association with FMRP would suggest an involvement of FMRP in translational regulation at the basal level and that FMRP could be an indicator of healthier neurons that maintain the rate of protein translation closer to normal levels.

Third, a reduction in SNAP25 coverage of NM cell bodies following cochlea removal is consistent with progressive cell loss of auditory ganglion neurons. Specifically, 31% and 74% of ganglion neurons die at 4 and 21 days after cochlea removal, respectively (Born & Rubel, 1985). The observed SNAP25 reduction presumably reflects auditory axon degeneration and endbulb synapse removal from the cell body of postsynaptic NM neurons. A similar reduction in perisomatic presynaptic terminals using the synaptic vesicle protein 2 as the marker was detected in the bushy cells of the mouse VCN at 1 week after cochlea ablation (Lu, Harris, & Rubel, 2007). In this study, the authors proposed a shift of excitatory synapses from the cell body to dendrites as suggested by unchanged amplitude of spontaneous miniature excitatory postsynaptic currents (mEPSCs) and a correlation between rise and decay times of mEPSCs which indicates dendritic filtering (Lu et al., 2007). Future studies with single cell analyses are needed to determine whether this synaptic shift indeed occurs in the NM and VCN. Alternatively, reduced peri-somatic SNAP25 coverage may be an indicator of presynaptic terminal modification instead of a net loss of terminals. This possibility is supported by reduced expression of the vesicular glutamate transporter 1 and smaller sized synaptic vesicles as induced by a 10-day period of monaural conductive hearing loss (earplugging) in young adult rats (Clarkson et al., 2016). Regardless, the negative correlation between peri-somatic SNAP25 coverage and postsynaptic FMRP level may, again, associate with the overall health status of NM neurons such that neurons with more FMRP have a stronger capability of removing or modifying inactive presynaptic innervation. Consistent with this possibility, transsynaptic influence of postsynaptic FMRP loss on development and maintenance of presynaptic terminals has been reported in *drosophila* neuromuscular junctions (Sears & Broadie, 2017) and in NM neurons (X. Wang et al., 2018).

Finally, we identified a dramatic reduction in gephyrin intensity of afferent-deprived NM neurons. This alteration may be a consequence of reduced inhibitory connectivity and/or compromised gephyrin expression, either of which implicates weakened inhibitory neurotransmission. Excitatory afferent influence on inhibitory transmission has been detected in several other sensory circuits. For example, several types of hearing loss, including that induced by cochlea ablation, compromise the inhibitory innervation from the MNTB to the lateral superior olive (Kapfer, Seidl, Schweizer, & Grothe, 2002; Sanes & Takacs, 1993; Takesian et al., 2009). Similarly, monocular deprivation results in inhibitory synapse loss and rearrangement in the visual cortex (van Versendaal et al., 2012). This influence may represent a form of homeostatic synaptic plasticity through which neurons adjust synaptic excitation and inhibition to maintain network stability (Turrigiano, 2012).

Afferent influence of gephyrin and FMRP are likely events that are independent of each other, as there is no evidence in support of a direct interaction between FMRP and gephyrin mRNAs (Darnell et al., 2011). In fact, shRNA-induced FMRP downregulation of NM neurons does not affect the level of synaptic gephyrin during development (X. Wang et al., 2018), suggesting that postsynaptic gephyrin expression and synaptic clustering may be independent of cell autonomous FMRP level. The positive correlation of FMRP with gephyrin intensity under both intact and deprived conditions may suggest that FMRP plays a role in homeostatic synaptic plasticity in the NM by controlling the number of inhibitory synapses per neuron. This possibility is supported by altered inhibitory connectivity in several regions of the FMRP knockout mouse brain (Contractor, Klyachko, & Portera-Cailliau, 2015). Specifically in the auditory brainstem, several cell groups including VCN show altered levels of antibody staining of inhibitory synaptic markers including vesicular GABA transporter, vesicular glycine transporter 2, and glutamate decarboxylase 67 in *Fmr1* knockout mice (McCullagh et al., 2020).

It remains to be determined whether the observed correlations of FMRP are pathological versus physiological. Some of the correlations (with cell body size and SNAP25) only appear in the deafferented condition, suggesting that a relationship depends on the pathology and does not occur normally. The correlations with gephyrin and Y10B hold in both intact and deafferented conditions, suggesting that these relationships may be more fundamental. Interestingly, the correlation between FMRP and gephyrin intensity is stronger in the afferent-deprived NM (R^2 = 0.46) compared with the intact side (R^2 = 0.18). This enhanced correlation between FMRP and gephyrin, along with the correlation between FMRP and SNAP25 emerged only after afferent deprivation, suggest that FMRP may play a more dramatic role in modulating the organization of neuronal circuits under certain manipulated or pathological conditions. The seemingly "mismatched" findings of FMRP correlation with SNAP25 and gephyrin (negative

vs. positive) should not be taken to assume that FMRP differentially regulates the two proteins or regulates excitatory versus inhibitory synapses, based on two reasons. First, our manipulation (cochlea removal) results in an immediate and complete elimination of excitatory afferent input to NM neurons (Born et al., 1991). It is not clear, however, how this manipulation affects inhibitory transmission to NM neurons. Second, any potential relationship between postsynaptic FMRP and presynaptic SNAP25 would be due to transsynaptic influence, while the relationship between FMRP and gephyrin in NM neurons may depend on cell autonomous interactions. Future studies of manipulating FMRP expression in NM/VCN neurons with either intact or deprived inputs are expected to help determine the exact role of FMRP in regulating neuronal integrity, long-term synaptic changes, and maintenance of the excitation/inhibition balance in response to changes in afferent inputs.

5 | CONCLUSION

Current understanding of FMRP function in the brain is largely derived from studies that characterize changes in neuronal properties and synaptic connectivity following FMRP loss or dysfunction. Results from this and other studies that manipulate sensory inputs and other environmental factors in FMRP wildtype cells and animals indicate that the normal functions of FMRP can be highly dynamic in ways associated with cellular and synaptic adjustments in response to changes in neuronal activity. In-depth functional characterization of normally expressed FMRP is significant, as FMRP is not only responsible for FXS but is also involved in several neurological and neurodegenerative disorders (Fatemi & Folsom, 2011; Tan et al., 2020). In addition, the dramatic and multiple forms of FMRP changes following afferent deprivation as revealed in this study may suggest a possible role of FMRP in hearing loss-induced brain alterations.

ACKNOWLEDGMENTS

This study was supported by the National Institute on Deafness and Other Communication Disorders (R01DC13074, R21DC17267, DC000018) and the United States—Israel Binational Science Foundation (2015087).

CONFLICT OF INTEREST

The authors declare no conflict of interest.

DATA AVAILABILITY STATEMENT

The data that support the findings of this study are available from the corresponding author upon reasonable request.

ORCID

Xiaoyan Yu https://orcid.org/0000-0002-4877-0114
Xiaoyu Wang https://orcid.org/0000-0003-2104-7089
Hitomi Sakano https://orcid.org/0000-0002-7471-8352
Diego A. R. Zorio https://orcid.org/0000-0003-1761-7878
Yuan Wang https://orcid.org/0000-0003-4347-7063

REFERENCES

Bartley, C. M., O'Keefe, R. A., Blice-Baum, A., Mihailescu, M. R., Gong, X., Miyares, L., … Bordey, A. (2016). Mammalian FMRP S499 is phosphorylated by CK2 and promotes secondary phosphorylation of FMRP. *eNeuro*, *3*(6), NEURO.0092. https://doi.org/10.1523/ENEURO.0092-16.2016

Bassell, G. J., & Warren, S. T. (2008). Fragile X syndrome: Loss of local mRNA regulation alters synaptic development and function. *Neuron*, *60*(2), 201–214. https://doi.org/10.1016/j.neuron.2008.10.004

Beebe, K., Wang, Y., & Kulesza, R. (2014). Distribution of fragile X mental retardation protein in the human auditory brainstem. *Neuroscience*, *273*, 79–91. https://doi.org/10.1016/j.neuroscience.2014.05.006

Boeynaems, S., Alberti, S., Fawzi, N. L., Mittag, T., Polymenidou, M., Rousseau, F., … Fuxreiter, M. (2018). Protein phase separation: A new phase in cell biology. *Trends in Cell Biology*, *28*(6), 420–435. https://doi.org/10.1016/j.tcb.2018.02.004

Born, D. E., Durham, D., & Rubel, E. W. (1991). Afferent influences on brainstem auditory nuclei of the chick: Nucleus magnocellularis neuronal activity following cochlea removal. *Brain Research*, *557*(1–2), 37–47. https://doi.org/10.1016/0006-8993(91)90113-a

Born, D. E., & Rubel, E. W. (1985). Afferent influences on brain stem auditory nuclei of the chicken: Neuron number and size following cochlea removal. *The Journal of Comparative Neurology*, *231*(4), 435–445. https://doi.org/10.1002/cne.902310403

Born, D. E., & Rubel, E. W. (1988). Afferent influences on brain stem auditory nuclei of the chicken: Presynaptic action potentials regulate protein synthesis in nucleus magnocellularis neurons. *The Journal of Neuroscience*, *8*(3), 901–919.

Buchan, J. R., & Parker, R. (2009). Eukaryotic stress granules: The ins and outs of translation. *Molecular Cell*, *36*(6), 932–941. https://doi.org/10.1016/j.molcel.2009.11.020

Call, C. L., & Hyson, R. L. (2016). Activity-dependent regulation of calcium and ribosomes in the chick cochlear nucleus. *Neuroscience*, *316*, 201–208. https://doi.org/10.1016/j.neuroscience.2015.12.042

Carzoli, K. L., & Hyson, R. L. (2011). In vivo analysis of the role of metabotropic glutamate receptors in the afferent regulation of chick cochlear nucleus neurons. *Hearing Research*, *272*(1–2), 49–57. https://doi.org/10.1016/j.heares.2010.10.020

Ceman, S., O'Donnell, W. T., Reed, M., Patton, S., Pohl, J., & Warren, S. T. (2003). Phosphorylation influences the translation state of FMRP-associated polyribosomes. *Human Molecular Genetics*, *12*(24), 3295–3305. https://doi.org/10.1093/hmg/ddg350

Clarkson, C., Antunes, F. M., & Rubio, M. E. (2016). Conductive hearing loss has long-lasting structural and molecular effects on presynaptic and postsynaptic structures of auditory nerve synapses in the Cochlear nucleus. *The Journal of Neuroscience*, *36*(39), 10214–10227. https://doi.org/10.1523/JNEUROSCI.0226-16.2016

Contractor, A., Klyachko, V. A., & Portera-Cailliau, C. (2015). Altered neuronal and circuit excitability in fragile X syndrome. *Neuron*, *87*(4), 699–715. https://doi.org/10.1016/j.neuron.2015.06.017

Darnell, J. C., Van Driesche, S. J., Zhang, C., Hung, K. Y., Mele, A., Fraser, C. E., … Darnell, R. B. (2011). FMRP stalls ribosomal translocation on mRNAs linked to synaptic function and autism. *Cell*, *146*(2), 247–261. https://doi.org/10.1016/j.cell.2011.06.013

Didiot, M. C., Subramanian, M., Flatter, E., Mandel, J. L., & Moine, H. (2009). Cells lacking the fragile X mental retardation protein (FMRP) have normal RISC activity but exhibit altered stress granule assembly. *Molecular Biology of the Cell*, *20*(1), 428–437. https://doi.org/10.1091/mbc.E08-07-0737

Doll, C. A., & Broadie, K. (2015). Activity-dependent FMRP requirements in development of the neural circuitry of learning and memory. *Development*, *142*(7), 1346–1356. https://doi.org/10.1242/dev.117127

Doll, C. A., Vita, D. J., & Broadie, K. (2017). Fragile X mental retardation protein requirements in activity-dependent critical period neural circuit refinement. *Current Biology*, *27*(15), 2318–2330 e2313. https://doi.org/10.1016/j.cub.2017.06.046

Fatemi, S. H., & Folsom, T. D. (2011). The role of fragile X mental retardation protein in major mental disorders. *Neuropharmacology*, *60*(7–8), 1221–1226. https://doi.org/10.1016/j.neuropharm.2010.11.011

Feng, Y., Gutekunst, C. A., Eberhart, D. E., Yi, H., Warren, S. T., & Hersch, S. M. (1997). Fragile X mental retardation protein: Nucleocytoplasmic shuttling and association with somatodendritic ribosomes. *The Journal of Neuroscience*, *17*(5), 1539–1547.

Francis, H. W., & Manis, P. B. (2000). Effects of deafferentation on the electrophysiology of ventral cochlear nucleus neurons. *Hearing Research*, *149*(1–2), 91–105. https://doi.org/10.1016/s0378-5955(00)00165-9

Gabel, L. A., Won, S., Kawai, H., McKinney, M., Tartakoff, A. M., & Fallon, J. R. (2004). Visual experience regulates transient expression and dendritic localization of fragile X mental retardation protein. *The Journal of Neuroscience*, *24*(47), 10579–10583. https://doi.org/10.1523/JNEUROSCI.2185-04.2004

Garden, G. A., Canady, K. S., Lurie, D. I., Bothwell, M., & Rubel, E. W. (1994). A biphasic change in ribosomal conformation during transneuronal degeneration is altered by inhibition of mitochondrial, but not cytoplasmic protein synthesis. *The Journal of Neuroscience*, *14*(4), 1994–2008.

Garden, G. A., Redeker-DeWulf, V., & Rubel, E. W. (1995). Afferent influences on brainstem auditory nuclei of the chicken: Regulation of transcriptional activity following cochlea removal. *The Journal of Comparative Neurology*, *359*(3), 412–423. https://doi.org/10.1002/cne.903590305

Hagerman, R. J., Berry-Kravis, E., Hazlett, H. C., Bailey, D. B., Jr., Moine, H., Kooy, R. F., … Hagerman, P. J. (2017). Fragile X syndrome. *Nature Reviews. Disease Primers*, *3*, 17065. https://doi.org/10.1038/nrdp.2017.65

Hashisaki, G. T., & Rubel, E. W. (1989). Effects of unilateral cochlea removal on anteroventral cochlear nucleus neurons in developing gerbils. *The Journal of Comparative Neurology*, *283*(4), 5–73. https://doi.org/10.1002/cne.902830402

Heil, P., & Scheich, H. (1986). Effects of unilateral and bilateral cochlea removal on 2-deoxyglucose patterns in the chick auditory system. *The Journal of Comparative Neurology*, *252*(3), 279–301. https://doi.org/10.1002/cne.902520302

Hong, H., Wang, X., Lu, T., Zorio, D. A. R., Wang, Y., & Sanchez, J. T. (2018). Diverse intrinsic properties shape functional phenotype of low-frequency neurons in the auditory brainstem. *Frontiers in Cellular Neuroscience*, *12*, 175. https://doi.org/10.3389/fncel.2018.00175

Hyson, R. L., & Rubel, E. W. (1995). Activity-dependent regulation of a ribosomal RNA epitope in the chick cochlear nucleus. *Brain Research*, *672*(1–2), 196–204. https://doi.org/10.1016/0006-8993(94)01390-4

Irwin, S. A., Christmon, C. A., Grossman, A. W., Galvez, R., Kim, S. H., DeGrush, B. J., … Greenough, W. T. (2005). Fragile X mental retardation protein levels increase following complex environment exposure in rat brain regions undergoing active synaptogenesis. *Neurobiology of Learning and Memory*, *83*(3), 180–187. https://doi.org/10.1016/j.nlm.2004.11.004

Irwin, S. A., Swain, R. A., Christmon, C. A., Chakravarti, A., Weiler, I. J., & Greenough, W. T. (2000). Evidence for altered fragile-X mental retardation protein expression in response to behavioral stimulation. *Neurobiology of Learning and Memory*, *74*(1), 87–93.

Jeon, S. J., Han, S. H., Yang, S. I., Choi, J. W., Kwon, K. J., Park, S. H., … Shin, C. Y. (2012). Positive feedback regulation of Akt-FMRP pathway protects neurons from cell death. *Journal of Neurochemistry*, *123*(2), 226–238. https://doi.org/10.1111/j.1471-4159.2012.07886.x

Jeon, S. J., Seo, J. E., Yang, S. I., Choi, J. W., Wells, D., Shin, C. Y., & Ko, K. H. (2011). Cellular stress-induced up-regulation of FMRP promotes cell survival by modulating PI3K-Akt phosphorylation cascades. *Journal of Biomedical Science*, *18*, 17. https://doi.org/10.1186/1423-0127-18-17

Kapfer, C., Seidl, A. H., Schweizer, H., & Grothe, B. (2002). Experience-dependent refinement of inhibitory inputs to auditory coincidence-detector neurons. *Nature Neuroscience*, *5*(3), 247–253. https://doi.org/10.1038/nn810

Kelley, M. S., Lurie, D. I., & Rubel, E. W. (1997). Rapid regulation of cytoskeletal proteins and their mRNAs following afferent deprivation in the avian cochlear nucleus. *The Journal of Comparative Neurology*, *389*(3), 469–483.

Kim, H., Gibboni, R., Kirkhart, C., & Bao, S. (2013). Impaired critical period plasticity in primary auditory cortex of fragile X model mice. *The Journal of Neuroscience*, *33*(40), 15686–15692. https://doi.org/10.1523/JNEUROSCI.3246-12.2013

Kim, H. K., Kim, Y. B., Kim, E. G., & Schuman, E. (2005). Measurement of dendritic mRNA transport using ribosomal markers. *Biochemical and Biophysical Research Communications*, *328*(4), 895–900. https://doi.org/10.1016/j.bbrc.2005.01.041

Kim, S. H., Dong, W. K., Weiler, I. J., & Greenough, W. T. (2006). Fragile X mental retardation protein shifts between polyribosomes and stress granules after neuronal injury by arsenite stress or in vivo hippocampal electrode insertion. *The Journal of Neuroscience*, *26*(9), 2413–2418. https://doi.org/10.1523/JNEUROSCI.3680-05.2006

Koenig, E., Martin, R., Titmus, M., & Sotelo-Silveira, J. R. (2000). Cryptic peripheral ribosomal domains distributed intermittently along mammalian myelinated axons. *The Journal of Neuroscience*, *20*(22), 8390–8400.

Kotak, V. C., Fujisawa, S., Lee, F. A., Karthikeyan, O., Aoki, C., & Sanes, D. H. (2005). Hearing loss raises excitability in the auditory cortex. *The Journal of Neuroscience*, *25*(15), 3908–3918. https://doi.org/10.1523/JNEUROSCI.5169-04.2005

Lerner, E. A., Lerner, M. R., Janeway, C. A., Jr., & Steitz, J. A. (1981). Monoclonal antibodies to nucleic acid-containing cellular constituents: Probes for molecular biology and autoimmune disease. *Proceedings of the National Academy of Sciences of the United States of America*, *78*(5), 2737–2741. https://doi.org/10.1073/pnas.78.5.2737

Lu, Y., Harris, J. A., & Rubel, E. W. (2007). Development of spontaneous miniature EPSCs in mouse AVCN neurons during a critical period of afferent-dependent neuron survival. *Journal of Neurophysiology*, *97*(1), 635–646. https://doi.org/10.1152/jn.00915.2006

Maurin, T., Zongaro, S., & Bardoni, B. (2014). Fragile X syndrome: From molecular pathology to therapy. *Neuroscience and Biobehavioral Reviews*, *46*(Pt 2), 242–255. https://doi.org/10.1016/j.neubiorev.2014.01.006

Mazroui, R., Huot, M. E., Tremblay, S., Boilard, N., Labelle, Y., & Khandjian, E. W. (2003). Fragile X mental retardation protein determinants required for its association with polyribosomal mRNPs. *Human Molecular Genetics*, *12*(23), 3087–3096. https://doi.org/10.1093/hmg/ddg335

McBride, E. G., Rubel, E. W., & Wang, Y. (2013). Afferent regulation of chicken auditory brainstem neurons: Rapid changes in phosphorylation of elongation factor 2. *The Journal of Comparative Neurology*, *521*(5), 1165–1183. https://doi.org/10.1002/cne.23227

McCullagh, E. A., Rotschafer, S. E., Auerbach, B. D., Klug, A., Kaczmarek, L. K., Cramer, K. S., … Wang, Y. (2020). Mechanisms underlying auditory processing deficits in fragile X syndrome. *The FASEB Journal*, *34*(3), 3501–3518. https://doi.org/10.1096/fj.201902435R

Mostafapour, S. P., Cochran, S. L., Del Puerto, N. M., & Rubel, E. W. (2000). Patterns of cell death in mouse anteroventral cochlear nucleus neurons after unilateral cochlea removal. *The Journal of Comparative Neurology*, *426*(4), 561–571. https://doi.org/10.1002/1096-9861(20001030)426:4<561::aid-cne5>3.0.co;2-g

Ocak, E., Eshraghi, R. S., Danesh, A., Mittal, R., & Eshraghi, A. A. (2018). Central auditory processing disorders in individuals with autism Spectrum disorders. *Balkan Medical Journal*, *35*(5), 367–372. https://doi.org/10.4274/balkanmedj.2018.0853

Pan, F., Aldridge, G. M., Greenough, W. T., & Gan, W. B. (2010). Dendritic spine instability and insensitivity to modulation by sensory experience in a mouse model of fragile X syndrome. *Proceedings of the National Academy of Sciences of the United States of America*, *107*(41), 17768–17773. https://doi.org/10.1073/pnas.1012496107

Penagarikano, O., Mulle, J. G., & Warren, S. T. (2007). The pathophysiology of fragile x syndrome. *Annual Review of Genomics and Human Genetics*, *8*, 109–129. https://doi.org/10.1146/annurev.genom.8.080706.092249

Price, D. K., Zhang, F., Ashley, C. T., Jr., & Warren, S. T. (1996). The chicken FMR1 gene is highly conserved with a CCT 5′-untranslated repeat and encodes an RNA-binding protein. *Genomics*, *31*(1), 3–12. https://doi.org/10.1006/geno.1996.0002

Sanes, D. H., & Takacs, C. (1993). Activity-dependent refinement of inhibitory connections. *The European Journal of Neuroscience*, *5*(6), 570–574. https://doi.org/10.1111/j.1460-9568.1993.tb00522.x

Sears, J. C., & Broadie, K. (2017). Fragile X mental retardation protein regulates activity-dependent membrane trafficking and trans-synaptic signaling mediating synaptic remodeling. *Frontiers in Molecular Neuroscience*, *10*, 440. https://doi.org/10.3389/fnmol.2017.00440

Sie, K. C., & Rubel, E. W. (1992). Rapid changes in protein synthesis and cell size in the cochlear nucleus following eighth nerve activity blockade or cochlea ablation. *The Journal of Comparative Neurology*, *320*(4), 501–508. https://doi.org/10.1002/cne.903200407

Steward, O., & Rubel, E. W. (1985). Afferent influences on brain stem auditory nuclei of the chicken: Cessation of amino acid incorporation as an antecedent to age-dependent transneuronal degeneration. *The Journal of Comparative Neurology*, *231*(3), 385–395. https://doi.org/10.1002/cne.902310308

Strumbos, J. G., Brown, M. R., Kronengold, J., Polley, D. B., & Kaczmarek, L. K. (2010). Fragile X mental retardation protein is required for rapid experience-dependent regulation of the potassium channel Kv3.1b. *The Journal of Neuroscience*, *30*(31), 10263–10271. https://doi.org/10.1523/JNEUROSCI.1125-10.2010

Takesian, A. E., Kotak, V. C., & Sanes, D. H. (2009). Developmental hearing loss disrupts synaptic inhibition: Implications for auditory processing. *Future Neurology*, *4*(3), 331–349. https://doi.org/10.2217/FNL.09.5

Tan, Y., Sgobio, C., Arzberger, T., Machleid, F., Tang, Q., Findeis, E., … Koeglsperger, T. (2020). Loss of fragile X mental retardation protein precedes Lewy pathology in Parkinson's disease. *Acta Neuropathologica*, *139*(2), 319–345. https://doi.org/10.1007/s00401-019-02099-5

Tierney, T. S., Russell, F. A., & Moore, D. R. (1997). Susceptibility of developing cochlear nucleus neurons to deafferentation-induced death abruptly ends just before the onset of hearing. *The Journal of Comparative Neurology*, *378*(2), 295–306. https://doi.org/10.1002/(sici)1096-9861(19970210)378:2<295::aid-cne11>3.0.co;2-r

Todd, P. K., & Mack, K. J. (2000). Sensory stimulation increases cortical expression of the fragile X mental retardation protein in vivo. *Brain Research. Molecular Brain Research*, *80*(1), 17–25. https://doi.org/10.1016/s0169-328x(00)00098-x

Todd, P. K., Malter, J. S., & Mack, K. J. (2003). Whisker stimulation-dependent translation of FMRP in the barrel cortex requires activation of type I metabotropic glutamate receptors. *Brain Research. Molecular Brain Research*, *110*(2), 267–278. https://doi.org/10.1016/s0169-328x(02)00657-5

Towers, E. R., Kelly, J. J., Sud, R., Gale, J. E., & Dawson, S. J. (2011). Caprin-1 is a target of the deafness gene Pou4f3 and is recruited to stress granules in cochlear hair cells in response to ototoxic damage. *Journal of Cell Science*, *124*(Pt 7), 1145–1155. https://doi.org/10.1242/jcs.076141

Tsang, B., Arsenault, J., Vernon, R. M., Lin, H., Sonenberg, N., Wang, L. Y., … Forman-Kay, J. D. (2019). Phosphoregulated FMRP phase separation models activity-dependent translation through bidirectional control of mRNA granule formation. *Proceedings of the National Academy of Sciences of the United States of America*, *116*, 4218–4227. https://doi.org/10.1073/pnas.1814385116

Turrigiano, G. (2012). Homeostatic synaptic plasticity: Local and global mechanisms for stabilizing neuronal function. *Cold Spring Harbor Perspectives in Biology*, *4*(1), a005736. https://doi.org/10.1101/cshperspect.a005736

van Versendaal, D., Rajendran, R., Saiepour, M. H., Klooster, J., Smit-Rigter, L., Sommeijer, J. P., … Levelt, C. N. (2012). Elimination of inhibitory synapses is a major component of adult ocular dominance plasticity. *Neuron*, *74*(2), 374–383. https://doi.org/10.1016/j.neuron.2012.03.015

Wang, X., Hong, H., Brown, D. H., Sanchez, J. T., & Wang, Y. (2017). Distinct neural properties in the low-frequency region of the chicken cochlear nucleus magnocellularis. *eNeuro*, *4*(2), ENEURO.0016. https://doi.org/10.1523/ENEURO.0016-17.2017

Wang, X., Zorio, D. A. R., Schecterson, L., Lu, Y., & Wang, Y. (2018). Postsynaptic FMRP regulates synaptogenesis in vivo in the developing Cochlear nucleus. *The Journal of Neuroscience*, *38*(29), 6445–6460. https://doi.org/10.1523/JNEUROSCI.0665-18.2018

Wang, Y., Cunningham, D. E., Tempel, B. L., & Rubel, E. W. (2009). Compartment-specific regulation of plasma membrane calcium ATPase type 2 in the chick auditory brainstem. *The Journal of Comparative Neurology*, *514*(6), 624–640. https://doi.org/10.1002/cne.22045

Wang, Y., Sakano, H., Beebe, K., Brown, M. R., de Laat, R., Bothwell, M., … Rubel, E. W. (2014). Intense and specialized dendritic localization of the fragile X mental retardation protein in binaural brainstem neurons: A comparative study in the alligator, chicken, gerbil, and human. *The Journal of Comparative Neurology*, *522*(9), 2107–2128. https://doi.org/10.1002/cne.23520

Weiler, I. J., Irwin, S. A., Klintsova, A. Y., Spencer, C. M., Brazelton, A. D., Miyashiro, K., … Greenough, W. T. (1997). Fragile X mental retardation protein is translated near synapses in response to neurotransmitter activation. *Proceedings of the National Academy of Sciences of the United States of America*, *94*(10), 5395–5400. https://doi.org/10.1073/pnas.94.10.5395

Zalfa, F., Achsel, T., & Bagni, C. (2006). mRNPs, polysomes or granules: FMRP in neuronal protein synthesis. *Current Opinion in Neurobiology*, *16*(3), 265–269. https://doi.org/10.1016/j.conb.2006.05.010

Zirpel, L., & Rubel, E. W. (1996). Eighth nerve activity regulates intracellular calcium concentration of avian cochlear nucleus neurons via a metabotropic glutamate receptor. *Journal of Neurophysiology*, *76*(6), 4127–4139. https://doi.org/10.1152/jn.1996.76.6.4127

Zorio, D. A., Jackson, C. M., Liu, Y., Rubel, E. W., & Wang, Y. (2017). Cellular distribution of the fragile X mental retardation protein in the mouse brain. *The Journal of Comparative Neurology*, *525*(4), 818–849. https://doi.org/10.1002/cne.24100

How to cite this article: Yu X, Wang X, Sakano H, Zorio DAR, Wang Y. Dynamics of the fragile X mental retardation protein correlates with cellular and synaptic properties in primary auditory neurons following afferent deprivation. *J Comp Neurol*. 2020;1–20. https://doi.org/10.1002/cne.24959